Wind-sand tunnel testing of surface-mounted obstacles: Similarity requirements and a case study on a Sand Mitigation Measure

Journal of Wind Engineering & Industrial Aerodynamics 214 (2021) 104653

Contents lists available at ScienceDirect

Journal of Wind Engineering & Industrial Aerodynamics

journal homepage: www.elsevier.com/locate/jweia

# Wind-sand tunnel testing of surface-mounted obstacles: Similarity requirements and a case study on a Sand Mitigation Measure

Lorenzo Raffaele [a,c,*], Jeroen van Beeck [a], Luca Bruno [b,c]

[a] von Karman Institute for Fluid Dynamics, Environmental and Applied Fluid Dynamics Department, Waterloosesteenweg 72, B-1640, Sint-Genesius-Rode, Belgium
[b] Politecnico di Torino, Department of Architecture and Design, Viale Mattioli 39, I-10125, Torino, Italy
[c] Windblown Sand Modeling and Mitigation Joint Research Group, Italy-France

ARTICLE INFO

*Keywords:*
Wind tunnel
Windblown sand
Morphodynamics
Similarity requirements
Sand Mitigation Measure

ABSTRACT

Windblown sand flow interacts with a number of surface-mounted human-built obstacles. The wind-sand flow perturbation and resulting morphodynamic response of the sand bed cannot be assessed in analytical terms. Therefore, wind-sand tunnel studies around scale physical models are often carried out. They should be driven by physical similarity theory based on dimensionless numbers referred to the whole multiphase and multiscale flow. However, similarity requirements cannot be fully satisfied under typical testing conditions and attention should be paid on the extent of the similarity relaxation. In this study, the background of wind-sand tunnel testing of surface-mounted obstacles is recalled by reviewing wind tunnel setups and similarity requirements. Then, a wind-sand tunnel campaign on a Sand Mitigation Measure is described and critically discussed. The setup dimensionless numbers are compared with statistics on those of past studies. The inescapable relaxation of similarity requirements is motivated by the test goals. The time evolution towards in-equilibrium conditions of both sand bed morphodynamics and sand transport is discussed. Finally, the results of engineering interest are described: the Sand Mitigation Measure sand trapping performance is assessed in dimensionless terms through the measurements of the incoming and outgoing sand concentration in air.

## 1. Introduction

Wind engineering is currently experiencing an increasing interest in windblown sand modelling and mitigation techniques. Windblown sand hazard affects a number of civil structures and infrastructures in desert and sandy coastal environments (Middleton and Sternberg, 2013), such as pipelines (Kerr and Nigra, 1952), industrial facilities (Alghamdi and Al-Kahtani, 2005), towns (Zhang et al., 2007), single buildings (Rizvi, 1989; Bofah and Al-Hinai, 1986), farms (Wang et al., 2010), roads (Redding and Lord, 1981), and railways (Bruno et al., 2018b). The wind flow interacts with surface-mounted obstacles of any kind inducing erosion, transport, and sedimentation of sand around them. This can induce detrimental effects such as the loss of functionality of the endangered structure or infrastructure, e.g. by precluding vehicular and pedestrian traffic, or even danger for users when structural failure is involved (see e.g. Raffaele and Bruno, 2019).

Within a pure modelling perspective, windblown sand belongs to the wider class of fluid-driven particulate transport (Lo Giudice et al., 2019), together with windblown snow. Furthermore, both windblown sand and windblown snow may result in the same effects on engineering structures and infrastructures (Tominaga, 2018). As a result, the modelling approaches are analogous and can include numerical simulations and full scale or reduced scale physical testing to replicate the wind flow, sand/snow flux, and the resulting morphodynamic evolution of the sand/snow bed.

The *numerical simulation* approach has dramatically increased in the last decades, particularly as regards windblown snow engineering applications (Tominaga and Stathopoulos, 2020). The numerical simulation of windblown sand processes is mainly carried out through the resolution of Eulerian–Lagrangian or fully Eulerian models coupling the wind flow aerodynamics and aeolian processes, i.e. erosion, transport, sedimentation, and consequent avalanching determining the morphodynamic evolution of the sand bed (Lo Giudice et al., 2019). Whilst Eulerian–Lagrangian models are computationally expensive, fully Eulerian models suit well to engineering applications which requires the modelling of large-scale processes (Lo Giudice and Preziosi, 2020). Numerical simulations allow to save time and cost by cutting the

* Corresponding author at: von Karman Institute for Fluid Dynamics, Environmental and Applied Fluid Dynamics Department, Waterloosesteenweg 72, B-1640, Sint-Genesius-Rode, Belgium.
*E-mail address:* lorenzo.raffaele@vki.ac.be (L. Raffaele).
*URL:* https://hypersmm.vki.ac.be/er/ (L. Raffaele).

https://doi.org/10.1016/j.jweia.2021.104653
Received 18 December 2020; Received in revised form 19 April 2021; Accepted 6 May 2021
Available online 12 May 2021

number of physical tests. However, they are still at their infancy given both modelling and numerical issues and shall be always validated on the basis of physical testing.

*In-situ full scale tests* are traditionally believed as the most reliable approach. They manage to overcome many of the shortcomings of scale tests. However, they are expensive, time-consuming, and subject to partially uncontrolled environmental setup conditions. As such, their application can result inconsistent with the time and cost requirements of the endangered infrastructure owners.

*Wind tunnel scale tests* including flying sand or other particles around surface-mounted obstacles were pioneered since the Sixties (Storm et al., 1962) and extensively undertaken in the following decades (e.g. Isyumov, 1971; Iversen, 1980; Rodrigo et al., 2012) as substitutes for rare and relatively recent climatic wind tunnels and real snow (e.g. Delpech et al., 1998; Liu et al., 2018). Wind tunnel tests allow to reproduce and visualize with higher accuracy and in a more controlled setup the spatial and temporal evolution of sand bed around specific geometries. Nevertheless, difficulties remains in the accurate measurement of wind-induced shear stresses at the sand bed and sand flux. Wind tunnel testing is almost entirely carried out at reduced geometric scale for both economic and practicality reasons (Simiu and Scanlan, 1996). This opens the door to physical similarity theory referred to the whole multiphase and multiscale flow.

Similarity requirements for wind tunnel simulation of erosion, transport, sedimentation processes of both sand and snow have been first introduced in the scientific reports of Storm et al. (1962) and Odar (1965), and later discussed by Isyumov (1971), Snyder (1972), Kind (1976), Iversen (1980), Anno (1984), and White (1996), amongst others. Given their dimensionless nature, similarity requirements hold regardless the nature of the fluid and the particle. As a result, they can be applied to different challenging particle transport phenomena, such as windblown snow (e.g. Zhou et al., 2014), subaqueous bedload (e.g. Pähtz et al., 2021), and even sand transport on Mars (e.g. Greeley et al., 1974). In general, similarity requirements cannot be fully satisfied under typical testing conditions due to the multiphase flow and the multiscale features of the problem ranging from the sand grain/snow flake to the obstacle characteristic lengths, and to the wind field scales, as pointed out in Sherman (2020). As such, the choice of the most appropriate set of reference scales for scaling (Kwok et al., 1992), and the inescapable relaxation of some similarity requirements (Isyumov and Mikitiuk, 1990) remain theoretical and technical open and challenging issues. While windblown snow drift modelling has continuously benefit from similarity theory (see e.g. Zhou et al., 2014), dimensionless similarity parameters have been somewhat overlooked in the majority of the recent literature on wind-sand tunnel test (see e.g. Luo et al., 2016; Wang et al., 2017, 2018), the recent study carried out by Tominaga et al. (2018) being a remarkable exception. In his recent inspirational perspective paper, Sherman (2020) explicitly recognizes and comments the challenges induced by wind tunnel scaling, even if they are not included among the six vexations to be addressed in the future of aeolian research. In this study, we aim at complementing Sherman's list by a 7th vexation about Wind-Sand Tunnel Tests (WSTTs) similarity.

The state-of-art of WSTTs of surface-mounted obstacles is critically discussed by proposing a novel categorization of their setups, and by distinguishing between setup similarity dimensionless numbers and resulting dimensionless metrics. Then, the wind tunnel test on a so-called Path Sand Mitigation Measure (SMM, interested readers can refer to Bruno et al., 2018b) is carried out as a case study. The study has both theoretical and practical aims: (i) highlighting and discussing the practical limitations of WSTTs in complying with similarity requirements, (ii) assessing the reaching of in-equilibrium conditions of both the sand bed morphodynamics and sand transport around the SMM, (iii) confirming the conjectured aerodynamic working principle of the SMM through the analysis of sand bed morphodynamics, (iv) assessing a dimensionless sedimentation coefficient to quantify the SMM sand trapping performance. The inescapable relaxation and mismatching of similarity requirements are critically discussed in the light of the goals above.

The paper is organized into four further sections. Section 2 briefly reviews and critically discuss the most common setups and similarity requirements for wind-sand tunnel tests of surface-mounted obstacles. In Section 3, the case study is introduced and the wind tunnel setup is outlined. Wind tunnel test results are discussed in Section 4. Finally, conclusions and perspectives are outlined in Section 5.

## 2. Background on wind-sand tunnel tests

WSTTs allow for the measurement of the sand flux as well as the morphodynamics of the sand bed around the tested obstacle as a function of time. In the following, past WSTTs are briefly reviewed by classifying their setup and by discussing most common similarity requirements.

### 2.1. Wind-sand tunnel setups: a new classification

A not necessarily exhaustive survey of WSTTs is discussed in the following. The survey is based on a total of 65 tests from 17 studies cited in this paper. The main findings are shown in Fig. 1. Since the pioneering applications by Iversen et al. (1990) and Hotta and Horikawa (1991), a growing number of WSTTs has been observed within the last decade (Fig. 1a) and it is expected to further increase in the coming years, covering both basic research and applications in engineering and geomorphology.

In the following, two novel categorizations of WSTTs are proposed, with respect to scale model types and setup conditions. WSTTs are carried out around three main *types of obstacle* (Fig. 1b):

1. non-erodible nominally 2D obstacles mounted on erodible sand beds, such as Path SMMs (Hotta and Horikawa, 1991; Zhang et al., 2010; Tsukahara et al., 2012; Xiao et al., 2015; Cheng et al., 2017; Wang et al., 2017, 2018; Chen et al., 2019), embankments (Zhang et al., 2014) and transverse dunes (Jiang et al., 2014);
2. non-erodible 3D obstacles mounted on erodible sand beds, such as cylinders and cubes (Iversen et al., 1990; Mochizuki et al., 2012; McKenna Neuman and Bédard, 2015; Luo et al., 2016; Tominaga, 2018);
3. erodible obstacles, such as sand dunes and piles (Faria et al., 2011; Ferreira and Fino, 2012).

Erodible obstacles or sand bed around them necessarily imply their initial shaping, not necessarily compliant to the actual erosion–transport–sedimentation balance. While fundamental studies can be also interested in the sand morphodynamic under transient non-equilibrium conditions, engineering applications are mainly interested in the response of the structure/infrastructure under (quasi) steady equilibrium conditions.

Therefore, a further and complementary WSTT categorization is proposed with respect to *setup conditions*. On the one hand, boundary conditions translate into the features of incoming sand flux $q_{in}$. On the other hand, initial conditions refer to the shape and volume of the sand bed surface set around the obstacle at the beginning of the test. The conditions above are expected to give rise to a different evolution of wind-sand state variables during the test, such as the sand flux, the shape and the volume of the sand bed around the obstacle. Fig. 1(c) categorizes the collected tests as a function of the adopted setup conditions. For the sake of clarity, Fig. 2 sketches each setup by providing the conjectured expected trend of the volume $V$ of the sand bed around the obstacle. It is worth stressing that the trend is purely qualitative and $V$ and related time intervals are out of scale for illustrative purposes only. $V$ varies during time $t$ from its initial value $V_0$ up to the equilibrium conditions. Two different equilibrium conditions are envisaged: equilibrium with concomitant incoming sand

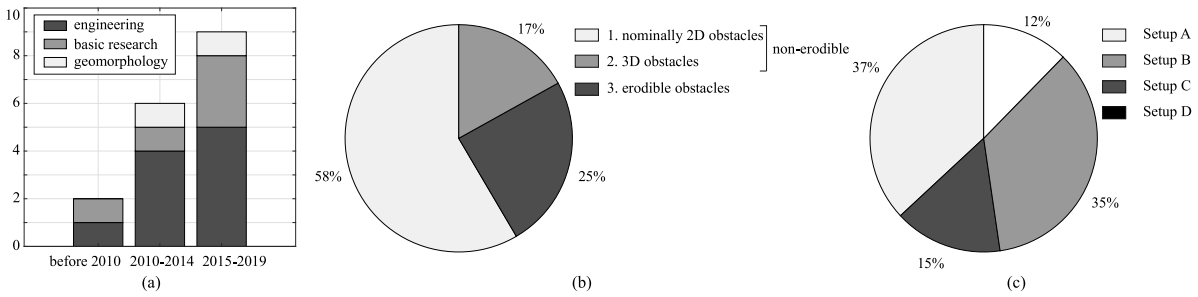


**Fig. 1.** Increasing trend of WSTTs in the literature (a), classification of WSTTs according to the nature of the tested obstacle (b) and setup conditions (c).

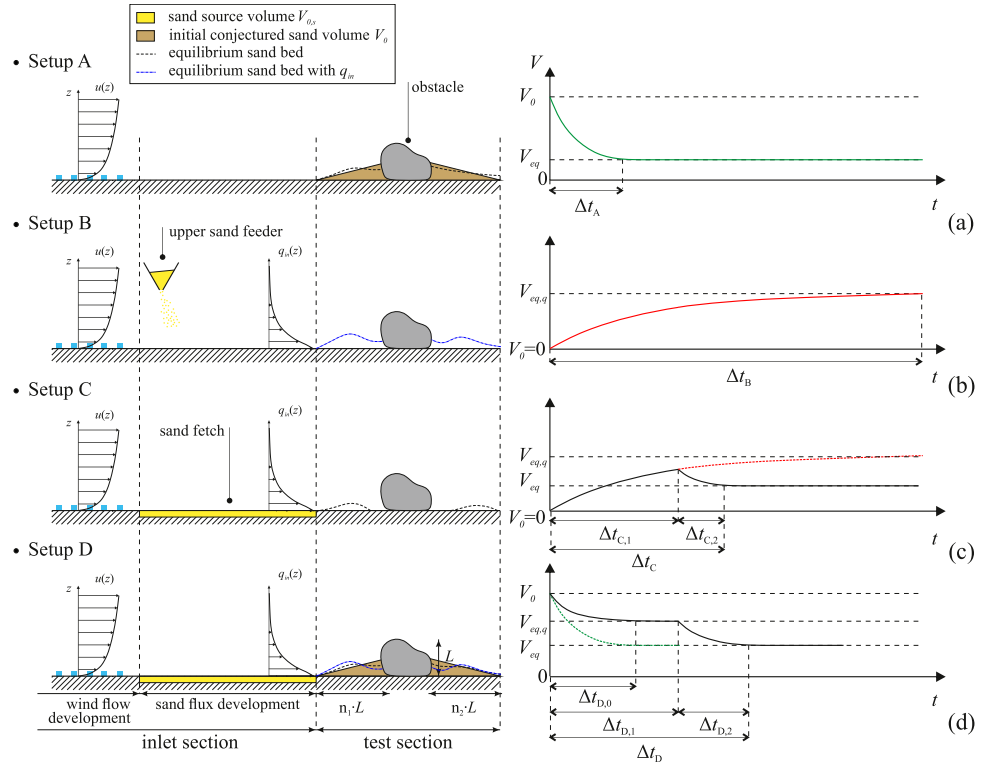


**Fig. 2.** WSTTs setups by varying boundary and initial conditions and related conjectured trend of the accumulated sand volume $V$.

transport, $V_{eq,q}$, and without concomitant incoming sand transport, $V_{eq}$. This is because transported sand subtracts momentum from the wind speed modifying the aerodynamics of the obstacle and the resulting morphodynamics, in turn. For each setup, the incoming wind flow features are supposed to be the same. In particular, the wind shear velocity $u_*$ is necessarily higher than the threshold one $u_{*t}$ in order to trigger windblown sand transport (Shao, 2008). In the following, each setup is briefly reviewed by identifying different expected regimes.

- Setup A implies a null sand flux boundary condition and a non-null sand bed initial condition around the obstacle. Given the out-of-equilibrium initial condition, $V$ modifies from the initial value $V_0$ to the in-equilibrium value $V_{eq}$ compliant with actual erosion regions induced around the obstacle, i.e. the regions where $|u_*| > u_{*t}$, within the transient regime spanning $\Delta t_A$. As such, it is expected that $V_{eq}$ and the time interval $\Delta t_A$ both depend on $V_0$. Setup A is often adopted in fundamental studies to investigate the transient sand bed morphodynamics starting from an horizontal initial conjectured sand level as it reaches the steady state (see e.g. Iversen et al., 1990; Faria et al., 2011; Ferreira and Fino, 2012; Mochizuki et al., 2012; Tsukahara et al., 2012; McKenna Neuman and Bédard, 2015).
- Setup B implies a non-null sand flux boundary condition and a null sand bed initial condition. In particular, it foresees the adoption of an upper sand feeder as sand supplier. The upper sand feeder has commonly two purposes. First, it guarantees that no depletion of sand source occurs during the test, i.e. $V_{0,s} = \infty$. Secondly, it is considered to mimic an infinite long upwind sand fetch allowing the simulation of a fully developed saltation layer (Carneiro et al., 2015). The sand progressively accumulates around the obstacle in the sedimentation regions, i.e. the regions where $|u_*| < u_{*t}$. The evolution of $V$ is expected to slowly tend to $V_{eq,q}$ within the time interval $\Delta t_B$. Setup B is the one that mostly allows to replicate real world conditions by testing the full progressive burying of the obstacle. However, the time interval $\Delta t_B$ required to reach equilibrium starting from $V_0 = 0$ is expected to be the longest among four setups since it depends solely on $q_{in}$. As a result, this setup is commonly adopted to investigate sand transport and sedimentation far from equilibrium (see e.g. Cheng et al., 2017; Chen et al., 2019).
- Setup C implies a non-null sand flux boundary condition and a null sand bed initial condition. It implements a uniform sand fetch upwind the test section as sand source. The sand fetch should be long enough to allow saltation to fully develop over

the length of the test section and reach equilibrium. However, this is impracticable in most wind tunnel tests since the minimum fetch length is expected to be approximately equal to 20 m (Shao and Raupach, 1992). From the null initial condition, $V$ will tend to $V_{eq,q}$ over the time interval $\Delta t_{C,1}$ required to deplete the sand fetch volume $V_{0,s}$. After that, $V$ will adjust to $V_{eq}$ to comply with $q_{in} = 0$ within a transient regime spanning $\Delta t_{C,2}$. As such, $V_{eq}$ as well as $\Delta t_C = \Delta t_{C,1} + \Delta t_{C,2}$ are expected to depend on both $V_{0,s}$ and $q_{in}$. The main drawback of this setup is the finite amount of sand supply which may not allow to reach $V_{eq,q}$. Setup C is commonly adopted to investigate sand transport and sedimentation far from equilibrium in analogy to Setup B (see e.g. Jiang et al., 2014; Zhang et al., 2014; Xiao et al., 2015; Luo et al., 2016; Wang et al., 2017, 2018).

- Setup D derives form the combination of Setup A and Setup C. It implements a sand fetch to induce $q_{in}$ together with a conjectured initial sand level. As such, it is expected that $V$ will tend to $V_{eq,q}$ within the time interval $\Delta t_{D,0}$, that is lower than $\Delta t_B$, following a trend analogous to the one of Setup A. However, it is worth stressing that this holds only if $\Delta t_{D,0}$ is lower than the time interval $\Delta t_{D,1}$ required to deplete $V_{0,s}$. After that, $V$ will adjust to $V_{eq}$ to comply with $q_{in} = 0$ within a transient regime spanning $\Delta t_{D,2}$. As a result, $\Delta t_D = \Delta t_{D,1} + \Delta t_{D,2} > \Delta t_A$. Setup D drastically simplifies the wind tunnel sand feeding system. Furthermore, it allows to shorten the testing time to investigate sand transport and morphodynamics for partial and complete covering of the obstacle. However, in the past literature, Setup D is commonly adopted with a conjectured sand level corresponding to the horizontal flat sand bed (see e.g. Hotta and Horikawa, 1991; Zhang et al., 2010; Tominaga, 2018).

The identified transient and quasi-steady regimes are induced by boundary and initial conditions, respectively. Hence, they are expected to vary substantially depending on the wind tunnel setup conditions. It is worth highlighting that the transient regime does not take place under in-field natural conditions since the conjectured sand level is an artificial initial condition.

As far as Path SMM are concerned, according to the authors, the setup choice shall be driven by the aim of the study. Setup A can be suitable to preliminary identify erosion/sedimentation zones around the obstacle analogously to wind tunnel sand erosion tests (Blocken et al., 2016) or RANS CFD simulations (see e.g. Bruno et al., 2018a). Setup B and C can be suited to assess sand transport and sedimentation regions around the clean obstacle, i.e. in the early stage of SMM installation. Finally, Setup D is the most suited for SMM performance assessment: if recursively carried out, it allows to efficiently investigate both morphodynamics and sand flux around the SMM under several conjectured sand levels, so to assess the discrete piece-wise varying sand trapping performance versus the accumulated sand volume.

### 2.2. Similarity requirements

The sand bed morphodynamics as well as the windblown sand transport surrounding the tested obstacle depend on several dimensionless parameters driving the physical similarity between model and prototype conditions. In general, they shall be matched both on *flat plane* (i.e. uniform sand fetch without any obstacle), and around the *surface-mounted obstacle*. Most common similarity requirements are herein briefly recalled from the literature of windblown sand and windblown snow branches of wind engineering by classifying them depending on the retained similarity features, namely geometry and kinematics of the wind-sand flow features. Then, relaxation criteria are discussed and setup similarity dimensionless numbers and resulting dimensionless metrics are distinguished.

#### 2.2.1. Geometric similarity

Geometric similarity shall be achieved by scaling identically the surface-mounted obstacle and the sand bed surrounding it. This translates into the geometric similarity of the ratio between the macroscopic scale, i.e. the model characteristic length scale $L$, and the microscopic scale, i.e. the sand grain characteristic length scale corresponding to the mean diameter $\bar{d}$. In formulas:

$$\frac{\bar{d}}{L} = const. \tag{1}$$

The model geometry downscaling influences two key wind tunnel setup parameters, i.e. the blockage ratio BR and the model aspect ratio AR. When BR is significant (e.g. BR $>$ 0.05) and/or AR is not preserved, the flow around the model is no more representative of the prototype conditions and physical similarity is not valid.

#### 2.2.2. Kinematic similarity

Given the multiphase nature of the flow, kinematic similarity shall take into account features of both wind flow and carried sand particles.

The similarity of *wind flow* is traditionally determined by the well-known Reynolds number Re. The correct simulation of the boundary layer separation around a surface-mounted obstacle, and the sand transport in turn, can be taken into account by reproducing the same aerodynamic regime, which means:

$$\frac{U L}{\nu} = const, \tag{2}$$

where $U$ is the characteristic wind speed at the height $L$, and $\nu$ is the air kinematic viscosity. However, it is worth stressing that sharp-cornered bluff bodies are insensitive to Re number in the supercritical regime and Re similarity criterion can be relaxed (Simiu and Scanlan, 1996). Some authors proposed additional criteria for flat plane conditions based on the roughness Reynolds number $\mathrm{Re}_*$:

$$\frac{u_* k_s}{\nu} = const, \tag{3}$$

where $k_s$ is the equivalent Nikuradse roughness. When the wind flow is fully rough ($\mathrm{Re}_* > 60 \div 90$, Blocken et al., 2007), $\mathrm{Re}_*$ number independence arises and $z_0/k_s$ is constant. However, during saltation the absorption of wind momentum by saltating particles is perceived by the flow above the saltation layer as an increment of the aerodynamic roughness. This is commonly taken into account through the so-called apparent roughness length $z_{0,s}$ (see e.g. Sherman and Farrell, 2008). Iversen (1981) highlighted the importance of the correct scaling between $z_{0,s}$ and $L$ on the basis of the well known Jensen's model law (Jensen, 1958):

$$\frac{z_{0,s}}{L} = const. \tag{4}$$

The similarity in motion of *carried sand particles* shall be achieved by scaling the acting forces during ejection and transport. The particle ejection similarity is achieved by matching the Shields number (i.e. the normalized threshold shear stress or threshold densimetric Froude number, see e.g. Kwok et al., 1992; Zhou et al., 2014), expressing the ratio of cohesive force to gravity, and the ratio of aerodynamic to cohesive force (Anno, 1984):

$$\frac{\rho}{\rho_p - \rho} \frac{u_{*t}^2}{g\bar{d}} = const, \tag{5}$$

$$\frac{u_*}{u_{*t}} = const, \tag{6}$$

where $\rho$ is the air density and $\rho_p$ is the particle density. Some variations of Eq. (5) and (6) have been proposed by replacing $u_*$ by $U$ and $\bar{d}$ by $L$. The similarity of airborne particles is based on two complementary criteria, i.e. the densimetric Froude number Fr expressing the ratio of inertial force to gravity, and the ratio of drag to inertial force (Kind, 1986):

$$\frac{\rho_p}{\rho_p - \rho} \frac{U^2}{Lg} = const, \tag{7}$$

$$\frac{\omega_s}{U} = const, \tag{8}$$

where $\omega_s$ is the terminal sedimentation velocity of a particle under equilibrium conditions. On flat plane, the Froude number is usually assessed by replacing $L$ by $\bar{d}$ (Isyumov and Mikitiuk, 1990; Kwok et al., 1992) or by the height of the wind tunnel test section $h_{wt}$. The latter corresponds to the so-called independence Froude number criterion. According to Owen and Gillette (1985) and White and Mounla (1991), if $h_{wt}$ is too small, wind flow blockage will occur. This would give rise to out of equilibrium saltation alongstream (due to not uniform $u_*$) and consequent inaccurate modelling of the saltation trajectories. According to Owen and Gillette (1985), a wind tunnel should be free of this detrimental effect if $U^2/h_{wt}g < 20$.

#### 2.2.3. Relaxation criteria

If geometric and kinematic similarity are fulfilled, prototype state variables can be directly inferred from model state variables and vice versa. However, it is common knowledge that their full compliance is impracticable in wind tunnel tests (Iversen, 1980). The great variety and numerousness of similarity requirements try to enclose any modelling scale, i.e. from macroscopic (e.g. dunes) to microscopic (e.g. ripples) features (White, 1996). As such, it is considered reasonable to relax similarity requirements related to scales which do not strongly affect the state variables of interest. For instance, similarity criteria related to microscopic flow features can be relaxed if the aim of the study is the modelling of sand accumulation drift geometry around the obstacle (Iversen, 1981). In the wake of this, several authors suggested that Eq. (1), (5), (7) are deemed not necessary for the simulation of sand and snow drifts (Kind, 1976; Anno, 1984; Peterka and Petersen, 1990; Kwok et al., 1992). According to Kind (1976), Fr scaling can be abandoned if saltation lengths (or heights) are not too large with respect to the characteristic horizontal (or vertical) length. Furthermore, Eq. (6) can be relaxed if $u_*/u_{*t} > 1.4$ and Eq. (3) does not represent a strict requirement according to Peterka and Petersen (1990) and Qiang et al. (2019), respectively.

In the same spirit, the similarity parameters reviewed above are combined to correlate model and prototype state variables for modelling sand drifts. Iversen (1981) and Delpech et al. (1998) highlighted the importance of the dimensionless transport rate:

$$\frac{\rho}{\rho_p}\frac{U^2}{Lg}\left(1 - \frac{U_t}{U}\right) = const. \tag{9}$$

However, it should be stressed that Eq. (9) holds only if $\Delta V/L^2 U \Delta t = const$, being $\Delta t$ the characteristic time scale.

#### 2.2.4. Time scale extrapolation

When modelling gross features of the wind-sand flow, such as sand drifts, the characteristic time scale can be extrapolated even if geometric and kinematic similarities are not fully met. According to Iversen (1980) and Anno (1984), a reliable estimation of the time scale $\Delta t$ is based on the conservation of the ratio of the accumulated sand volume $\Delta V$ around the tested model to the reference volume $L^3$. Iversen (1980) combined Eq. (1), (5), (6), (9) into the so-called dimensionless transport rate roughness parameter:

$$\left(\frac{\Delta V}{L^3}\right)\left[\frac{\rho}{\rho_p}\frac{u_{*t}^2}{Lg}\left(\frac{U}{U_t}\right)^2\right]^{3/7}\left[\frac{\rho}{\rho_p}\frac{U^2}{Lg}\left(1 - \frac{U_t}{U}\right)\frac{U\Delta t}{L}\right]^{-1} = const. \tag{10}$$

Conversely, Anno (1984) proposed a simpler criterion based on the trapping capacity of the tested obstacle:

$$\frac{Q_{in}\eta\Delta t}{\rho_b L^2} = const, \tag{11}$$

where $Q_{in}$ is the incoming transport rate on flat plane, $\rho_b$ is the particle bulk density and $\eta$ is the so-called collection coefficient of the obstacle, so that $\Delta V = Q_{in}\eta\Delta t L/\rho_b$. However, according to the authors, each of the above equations shows some deficiencies. On the one hand, Eq. (10) results from the empirical fitting to data from model-scale and full-scale experiments of the same class of problems. As such, it is conditioned to a specific dataset. On the other hand, although Eq. (11) results from general theoretical assumptions, it requires the a priori non-trivial estimation of $\eta$.

#### 2.2.5. Setup and resulting dimensionless numbers

The reviewed dimensionless numbers are summarized in Table 1 according to similarity class, physical modelling aim, equation and main source. According to the authors, they can be categorized into two main categories, namely *setup dimensionless numbers* and *resulting dimensionless metrics*. On the one hand, setup dimensionless numbers result from wind tunnel setup parameters that are directly controllable, i.e. $L$, $d$, $z_0$, $U$. On the other hand, resulting dimensionless metrics result from wind-sand flow arising quantities somehow related to setup parameters, i.e. $k_s$, $z_{0,s}$, $u_{*t}$, $\omega_s$. In principle, such resulting metrics can be estimated through existing semi-empirical laws. However, they are affected by a number of uncertainties. In particular:

- to the authors' best knowledge, the sand grain roughness $k_s$ and the relation between $\mathrm{Re}_*$ and $z_{0,s}$ during saltation are slightly investigated. According to Kind (1976), the effects of viscosity on the flow are fairly small if $\mathrm{Re}_* > 20$ and the sand-grain roughness during saltation is equal to $k_s = 1/1.6(u_*^2/2g)$. However, the above estimate of $k_s$ are based on the debated Owen's hypothesis (see e.g. Pähtz et al., 2012).
- several laws have been proposed to directly assess $z_{0,s}$ on the basis of $u_*$ (e.g. Owen, 1964; Charnock, 1955; Sherman and Farrell, 2008). However, according to Sherman and Farrell (2008), none of the proposed laws returns proper values of $z_{0,s}$. Furthermore, $z_{0,s}$ is usually smaller in the wind tunnel than in the field of about one order of magnitude. Hence, the application of a universally valid equation seems questionable.
- several laws have been proposed to directly assess $u_{*t}$ (e.g. Bagnold, 1941; Shao and Lu, 2000; McKenna Neuman, 2003) and $\omega_s$ (e.g. Farrell and Sherman, 2015) as a function of $d$. However, $u_{*t}$ and $\omega_s$ are affected by a number of uncertainties. The authors attempted to statistically assess their variability in Raffaele et al. (2016) and Raffaele et al. (2020).

According to the authors, such shortcomings imply that the above-mentioned resulting dimensionless metrics are not strictly controllable through semi-empirical laws and, when possible, they should be assessed by direct measurements through preliminary tests aimed at characterizing the sand flux on flat plane conditions without any obstacle.

## 3. Layout of the experimental case study

The experimental case study is carried out on the Path SMM Shield for Sand (S4S). In the following, the tested Path SMM conceptual design and aerodynamic working principles are briefly provided. Then, the wind tunnel setup, scaling criterion, and measurement apparatus are discussed.

### 3.1. Tested path SMM

Shield for Sand is a patented, aerodynamically shaped solid barrier (Bruno et al., 2016). Its conceptual design is illustrated in Fig. 3.

S4S cross-section geometry is composed by three elements: (A) a foundation, (B) a lower quasi-vertical wall, and (C) an upper windward concave wind deflector (see Fig. 3a). Each component ensures a specific functional requirement of the SMM. The foundation defies the overturning moment induced by the lateral wind load and the upwind trapped sand passive pressure. The lower wall allows an easy sand removal maintenance by means of sand removal machines, e.g. sand ploughs or

**Table 1**
Similarity dimensionless numbers for WSTTs.

| Similarity class | Physical modelling | Similarity requirement | Equation | Source |
|---|---|---|---|---|
| Geometric | Wind flow | Length scale ratio | (1) | White (1996) |
| | | Blockage ratio | – | Simiu and Scanlan (1996) |
| | | Aspect ratio | – | |
| Kinematic | Wind flow | Reynolds number | (2) | White (1996) |
| | | Roughness Reynolds number | (3) | Kind (1976) |
| | | Apparent roughness length | (4) | Iversen (1981) |
| | Particle ejection | Shields number | (5) | Iversen (1981) |
| | | effective shear velocity | (6) | Anno (1984) |
| | Particle transport | Froude number | (7) | Kind (1986) |
| | | drag–inertia ratio | (8) | |
| – | Sand drift | Transport rate | (9) | Iversen (1981) |
| | | Transport rate roughness | (10) | Iversen (1980) |
| | | Trapped volume | (11) | Anno (1984) |

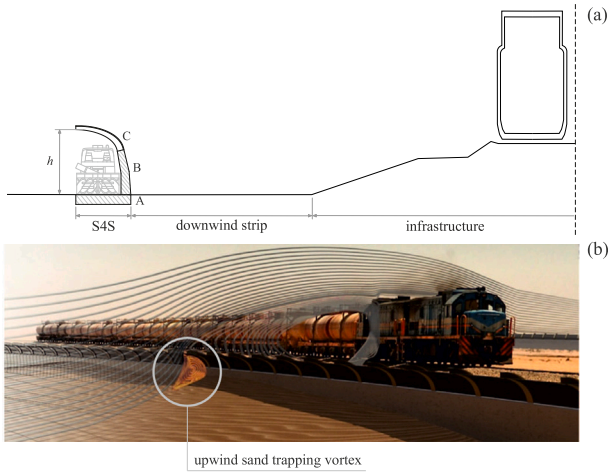


**Fig. 3.** Shield for Sand conceptual design (a) and aerodynamic working principle (b). Reprinted from Horvat et al. (2020) with permission from Elsevier.

sand blowers. The upper deflector ensures the S4S aerodynamic working principle: it induces an upwind recirculation vortex that promotes the local downward deflection of the wind flow and reverses the flow close to the ground, decreasing $u_*$. As a result, sand sedimentation occurs upwind the barrier where $|u_*| < u_{*t}$ preventing most of the sand from reaching the protected infrastructure downwind (Bruno et al., 2018a) . In light of this, the upwind recirculation region is defined as sand trapping vortex (see Fig. 3b).

### 3.2. Wind tunnel facility

The wind tunnel test is carried out in the wind tunnel L-1B of von Karman Institute for Fluid Dynamics. The facility is a closed-circuit wind tunnel with a test section length of about 20 m, and a cross-section of height $h_{wt} = 2$ m and width $w_{wt} = 3$ m. The tested model of height $h$ has been installed at the distance $a = 53.3h$ from the inlet of the test section while the sand fetch spans $c = 9.7h$ just upwind the tested model (see Fig. 4a).

A low-roughness boundary layer is set in order to simulate open terrain conditions, typical for sand deserts, by placing a monoplane grid with a mesh size of $0.02 \times 0.02$ m and a 0.15 m high fence at the inlet of the test section with no roughness elements. The reference wind velocity $U$ is measured at the inlet of the test section via Prandtl pitot tube. Some exploratory tests have been performed with empty wind tunnel test section and uniform sand layer to detect saltating grains via Particle Tracking Velocimetry (PTV) technique and ascertain the steadiness of the saltation layer. $U$ is set in order to induce a steady, fully developed saltation layer. The corresponding mean velocity profile $u(z)$ and mean turbulence intensity $I_u$ at the distance $a$ from the inlet without sand fetch is then measured via Particle Image Velocimetry (PIV) technique adopting a smoke generator to seed the flow with oil particles ranging from 1e-3 mm to 5e-3 mm. Fig. 4(b) shows the reproduced mean wind speed profile. The measurements are fitted with the log-law $u(z) = u_*/k \cdot \ln(z/z_0)$. The corresponding profile of the streamwise turbulence intensity $I_u$ is shown in Fig. 4(c). The measurements are fitted with $I_u(z) = (c_t \cdot \ln(z/z_0))^{-1}$, so that $c_t = 0.66$ (EN 1991-1-4, 1991).

Key wind tunnel facility setup parameters are summarized in Table 2 for the sake of clarity.

### 3.3. Wind-sand setup

The scale model of S4S is subdivided into three spanwise components: one short central transparent section, and two side non-transparent sections (see Fig. 5a). The central transparent section is fixed to the side sections and allows measurements below the concave deflector. The side sections are made of wood and aluminium to withstand the wind-induced pressure. Their purpose is to increase the model aspect ratio to reduce the edge effect caused by the interaction between the sand trapping vortex induced by S4S and the boundary layers on the side walls of the wind tunnel. The resulting model aspect ratio is equal to $AR = s/h = 6.23$. Two end plates are placed next to the lateral free-ends of the barrier to reduce end-tip aerodynamic effects and confine the upwind sand fetch.

The wind-sand tunnel Setup D is implemented (see Section 2.1). Six tests have been performed by setting up different initial conditions of accumulated sand in order to simulate the progressive filling of the barrier (see Fig. 5b): from level $l_0$ (i.e. no sand accumulated) to level $l_5$ (i.e. maximum simulated level of accumulated sand). Each level is set with an upwind slope angle $\alpha_u$ close to the natural one (e.g. Lancaster, 1995). A uniform sand fetch is spread upwind the barrier before each test as sand supplier. As a result, each test run is stopped as soon as an eroded sand patch is identified on the upwind fetch at $t = T$. This is to avoid unintended variations on the incoming sand flux due to the lack of erodible sand. The test on each sand accumulation level is performed twice to ascertain its repeatability.

The tested sand granulometry distribution is plotted in Fig. 6 through its cumulative distribution $F(d)$. The threshold shear velocity is estimated for flat plane conditions without the S4S model installed. Wind speed is gradually incremented until erosion is detected, i.e. $u_* = u_{*t}$, and the wind velocity profile is acquired via PIV technique. The measured value of the threshold shear velocity is low if compared with other wind tunnel measurements (see e.g. Raffaele et al., 2016). The authors conjecture that the obtained value can be the result of the very broad distributed sand granulometry and the presence of interspersed finer particles among coarser ones, reflected by the positively skewed distribution.

Key wind-sand setup parameters are summarized in Table 2 for the sake of clarity.

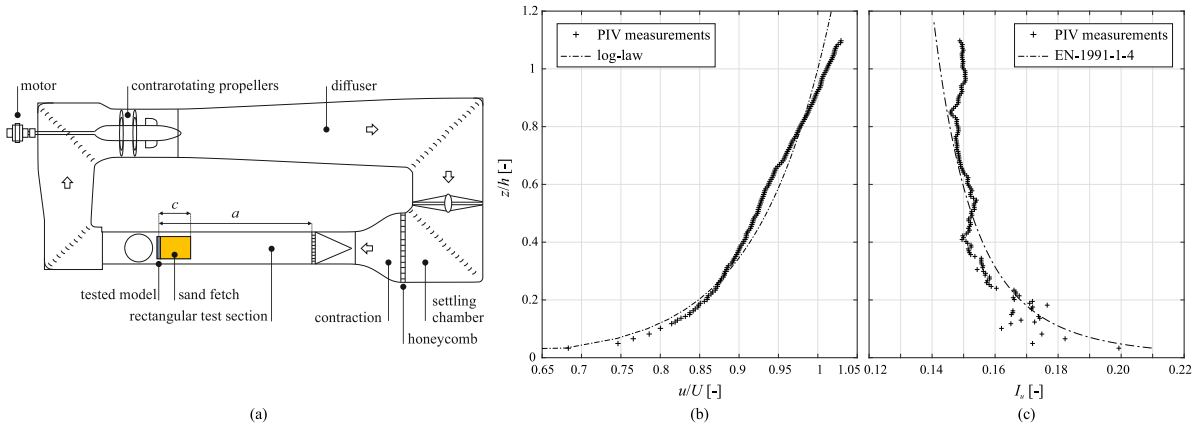


**Fig. 4.** Plan view of the L-1B wind tunnel (a), reproduced mean wind speed profile (b) and turbulence intensity profile (c).

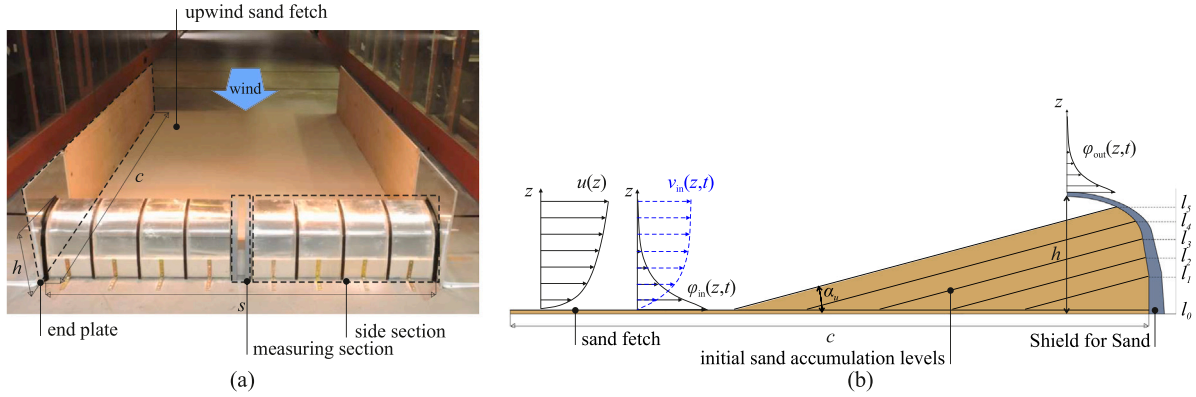


**Fig. 5.** Wind tunnel test setup (a) and scheme of the measuring cross-section for increasing initial sand accumulation levels (b).

**Table 2**
WSTT setup parameters.

| | | Setup parameter | Value |
|---|---|---|---|
| Wind tunnel facility | Test section | Height | $h_{wt} = 2$ m |
| | | Width | $w_{wt} = 3$ m |
| | Boundary layer | Reference wind speed | $U = 8.5$ m/s |
| | | Shear velocity | $u_* = 0.3$ m/s |
| | | Aerodynamic roughness | $z_0 = 3.5e-6$ m |
| | | Turbulence intensity | $I_u(h) = 0.15$ |
| Wind-sand setup | Model | Height | $h = 0.3$ m |
| | | Span | $s = 1.87$ m |
| | | Scale ratio | 1:10 |
| | Sand fetch | Length | $c = 2.9$ m |
| | | Thickness | $l_0 = 0.01$ m |
| | Initial conditions | Upwind slope angle | $\alpha_u = 15°$ |
| | | Sand level heights | $l_{1,\dots,5}/h = \{0.31,0.47,0.63,0.78,0.91\}$ |
| | | Test duration | $T = 850 - 1575$ s |
| | Sand characteristics | Mean diameter | $\bar{d} = 3.4e-4$ m |
| | | Threshold shear velocity | $u_{*t} = 0.15 \pm 0.02$ m/s |

### 3.4. Similarity requirements

The wind tunnel test is designed by referring to in-field prototype typical sand deserts conditions. The following prototype features of the geometry and wind flow are considered: an open-field roughness length $z_0 = 4e\text{-}3$ m; a mean threshold shear velocity $u_{*t} = 0.29$ m/s corresponding to the common mean grain diameter $\bar{d} = 0.25$ mm (Raffaele et al., 2016); a wind shear velocity higher than the threshold and equal to $u_* = 1.5u_{*t}$; a characteristic height equal to $h = 3$ m.

In the present study, similarity requirements relaxation is driven by the specific test goals. On the one hand, the simulation of sand drifts upwind the barrier presumes that similarity criteria related to large-scale features of the wind-sand flow shall be retained. On the other hand, the correct reproduction of the barrier's performance is assumed to be also sensitive to the small-scale features of the windblown sand flow, such as the scaling of the particles trajectory, herein expressed by the ratio between the saltation layer height $\delta_s$ and the barrier height $h$. In fact, given the correct scaling of the wind flow around the barrier, the incoming sand flux shall be geometrically scaled in analogy to the incoming wind speed profile by retaining the resulting dimensionless metric $\delta_s/h = const$.

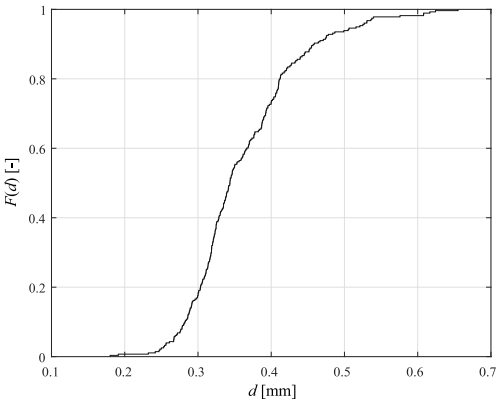


**Fig. 6.** Cumulative distribution of sand granulometry.

The scaling of $\delta_s$ is still object of study in the literature. Pioneering studies suggest $\delta_s$ scales with $u_*$ (Zingg, 1953; Owen, 1964). However, according to the more recent studies $\delta_s$ is expected do be slightly sensitive or fully insensitive to wind speed (Kok et al., 2012; Ho et al., 2014), to be much larger in the field rather than in wind tunnel tests and to be related to the median sand particle diameter (Martin and Kok, 2017). As such, the saltation layer height is hardly controllable in the wind tunnel. Under typical in-field conditions, it is expected $\delta_s/h \approx 0.05$, by considering a typical in-field saltation height equal to $\delta_s = 0.15$ m. As a result, the minimization of the discrepancy of the resulting dimensionless metric $\delta_s/h$ between model and prototype leaves no choice than play on the height of the model. Nonetheless, the model $h$ should fulfil other similarity requirements, namely the setup dimensionless numbers $d/L$, Re, and Fr, governing the similarity of geometry, wind flow and particle trajectory, always by taking into account BR and AR.

In Fig. 7, the model similarity dimensionless parameters from the present case study and past wind tunnel studies (see Section 2.1) are compared by referring to the same abovementioned prototype conditions. This is because in-field prototype conditions are seldom reported in the literature. In Fig. 7(a), the generic model setup dimensionless numbers $\phi_m$ are normalized with respect to the corresponding prototype dimensionless numbers $\phi_p$. The generic normalized similarity parameter is defined as $\phi^* = \phi_m/\phi_p$. Similarly, Fig. 7(b) plots the dispersion of BR and AR. In particular, AR is plotted only for nominally two-dimensional obstacles. The dispersion of $\phi^*$, BR and AR is synthetically represented by means of box plots. Fig. 7(c, d) shows the cardinality # of the wind tunnel tests taken into account in the estimation of each box plot. The discrepancies in cardinality are due to the omission of specific experimental setup parameters in some studies.

On the one hand, the closer $\phi^*$ is to 1, the closer the matching between model and prototype conditions is. On the other hand, low values of BR are recommended in general and high values of AR are preferable for Path SMM in order to limit and circumscribe end-tips aerodynamic effects, given their nominal 2D geometry. The collected setup dimensionless numbers allow to draw some general comments in a design perspective.

- Geometric similarity is impossible to be matched in wind-sand tunnel experiments (White, 1996). Indeed, the resulting downscaling of the particle diameter would require the adoption of dust particles. As such, this would give rise to strong interparticle forces, not physically sound for sand (see e.g. Raffaele et al., 2016). As a result, $u_{*t}$ and $\delta_s$ cannot be scaled with respect to the corresponding prototype values since they directly result from $d$. In turn, $u_*$ cannot be scaled since it must be larger than $u_{*t}$ to trigger saltation. Past wind tunnel studies confirm that $d/L$ is inescapably overestimated on average by a factor 5e+1.

**Table 3**
Dimensionless numbers of wind tunnel setup.

| Similarity class | Similarity requirement | Expression | $\phi^*$ | $\phi_m$ |
|---|---|---|---|---|
| Geometric | Length scale ratio | $\bar{d}/h$ | 15.84 | 1.32e−3 |
| | Blockage ratio | $sh/w_{wt}h_{wt}$ | – | 0.09 |
| | Aspect ratio | $s/h$ | – | 6.23 |
| Kinematic | Reynolds number | $hU/\nu$ | 0.12 | 1.73e+5 |
| | Shields number | $(\rho/\rho_p - \rho)(u_{*t}^2/g\bar{d})$ | 0.41 | 2.7e−3 |
| | Effective shear velocity | $u_*/u_{*t}$ | 1.34 | 2.01 |
| | Froude number | $U^2/hg$ | 14.43 | 25 |
| | Wind tunnel Froude number | $U^2/h_{wt}g$ | – | 3 |

- Froude number overestimation is inevitable since $U$ in model and prototype conditions is of the same order of magnitude. On the other side, Re underestimation is intrinsically bound to Fr overestimation due to the sharp conflict between Reynolds and Froude scaling. Past wind tunnel studies confirm that Fr number is inescapably overestimated on average by a factor 6e+1 while Re number is underestimated by a factor 3e-2.
- The proposed wind tunnel test setup results in $\phi^*$ values much closer to the unity than the vast majority of past studies. This is made possible by the large wind tunnel cross-section, which is the largest one adopted in WSTTs, to the authors' best knowledge. This allows to increase $h$ by complying with BR and AR. However, the need of minimizing $\delta_s/h$ leads a relatively high blockage ratio approximately equal to the third quartile, and to an aspect ratio lower than the median and about equal to the first quartile.

Overall, the collected setup dimensionless numbers highlight that a perfect matching of similarity requirements remains impracticable in conventional wind tunnel facilities. For the sake of completion, the case study dimensionless numbers are summarized in Table 3 through the similarity parameter $\phi^* = \phi_m/\phi_p$ and the model dimensionless parameter $\phi_m$.

### 3.5. Measurement apparatus

The installed measuring equipment allows for the detection of the morphodynamic evolution of the sand bed accumulated upwind the barrier, the incoming instantaneous sand particles concentration $\varphi_{in}(z,t)$ and velocity $v_{in}(z,t)$ over the flat sand bed, and the instantaneous outgoing sand concentration $\varphi_{out}(z,t)$ that overcomes the top of the barrier. The instantaneous outgoing particles velocity is impracticable to be assessed via standard non-time-resolved PTV due to the high intermittency of saltating particles over the barrier. As such, it is not evaluated in the present study. Each measurement is taken along the test section centreline and in correspondence of the measuring model section so that end-tip aerodynamic effects and influence of boundary layer developed on the lateral sides of the wind tunnel are minimized. A 200 mJ Nd:YAG laser source pulsating at 2 Hz is located on the ceiling of the testing chamber. A 3 mm width laser sheet is generated along the test section centreline and perpendicular to the floor. Two CMOS cameras with resolution 2360 × 1776 pixels are located outside the wind tunnel. Their Field of View (FoV) are sketched in Fig. 8(a). The velocity and concentration fields of incoming sand particles without the barrier installed as well as the morphodynamic evolution of the sand bed upwind the barrier highlighted by the pulsed-laser sheet are captured through a 24 mm objective ensuring a 85 × 60 cm Field of View (FoV #1, Fig. 8b). The same camera is used to measure the incoming wind speed via PIV. The concentration fields of outgoing sand particles are captured through a 35 mm objective ensuring a 50 × 50 cm Field of View (FoV #2, Fig. 8c).

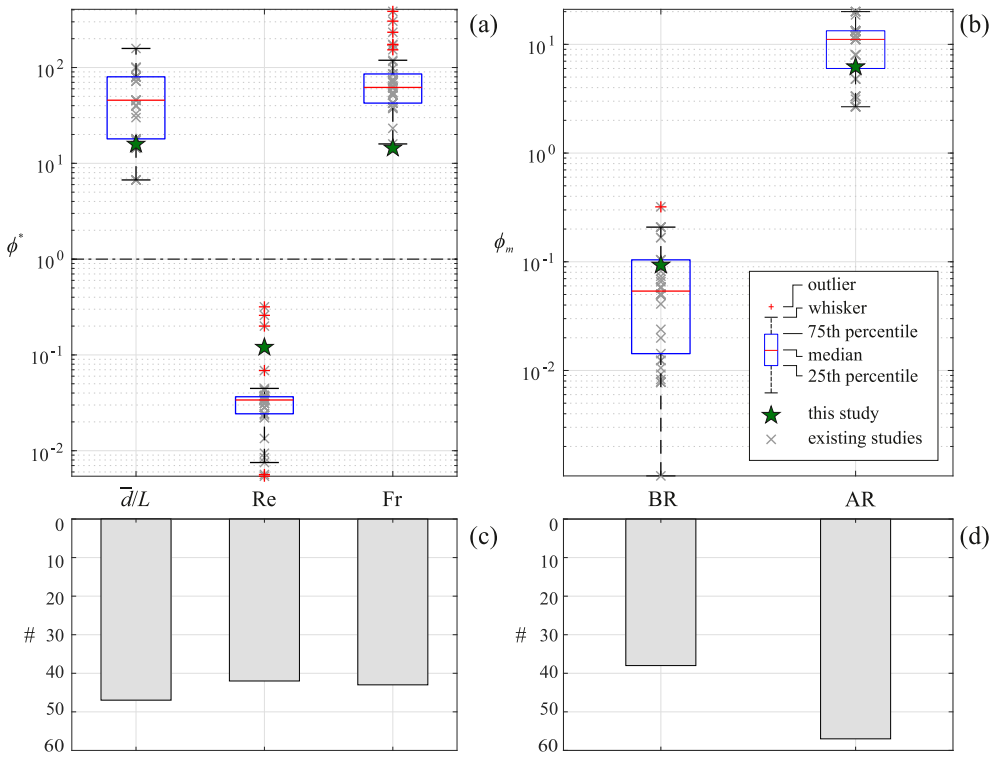


**Fig. 7.** Setup dimensionless numbers: similarity dimensionless numbers (geometry, Reynolds and Froude) normalized to prototype conditions (a), model blockage ratio BR and aspect ratio AR (b) and corresponding cardinality # of examined studies (c,d).

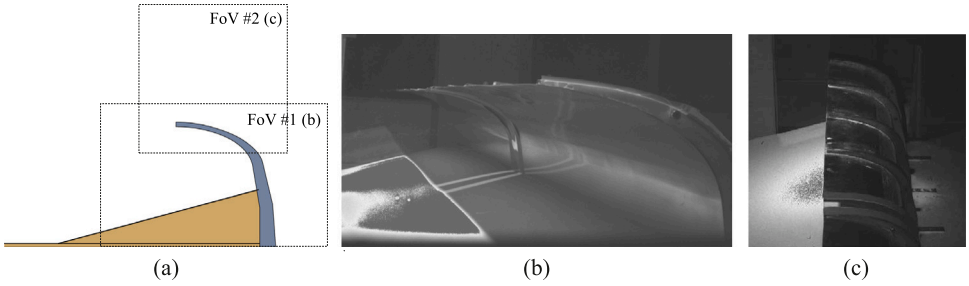


**Fig. 8.** Field of Views (FoVs) for PIV and PTV measurements: reference scheme (a), FoV #1 (b), and FoV #2 (c).

## 4. Results

In the following, the time convergence of wind-sand state variables is assessed through a preliminary analysis, then sand bed morphodynamics and sand transport around the barrier is discussed. Finally, the sand trapping performance is evaluated. It is worth stressing that the results discussed below refer to the similarity dimensionless numbers provided in Section 3.4 and cannot be a-priori generalized to other values of setup parameters.

### 4.1. Preliminary analysis

The time evolution of sand bed morphodynamics and sand concentration volume fraction $\varphi$ are preliminarily analysed in order to assess the reaching of in-equilibrium conditions. By way of example, Fig. 9 shows the time evolution of the sand bed together with the simultaneous outgoing bulk concentration $\Phi_{out}(t) = \int_h^\infty \varphi_{out}(z,t)\,dz$ normalized to the mean outgoing bulk concentration $\mu(\Phi_{out}) = 1/T \int_0^T \int_h^\infty \varphi_{out}(z,t)\,dz\,dt$ related to the sand level $l_1$, being $T$ the test duration. Fig. 9(a) plots the normalized elevation of the sand bed $z/h$ with a sampling interval $\Delta t_j$ = 5e+1 s, while Fig. 9(b) plots the normalized ratio $\Phi_{out}/\mu(\Phi_{out})$ with a sampling interval $\Delta t_k$ = 5e-1 s. Such features are plotted as a function of the time $t$ and the dimensionless time $t^* = tU/h$.

While the sand bed morphodynamics clearly reflects the transient regime and the progressive evolution towards in-equilibrium conditions, the wide fluctuations and intermittency of $\Phi_{out}$ hide the general trend of the sand concentration over the top of the barrier. In order to quantitatively assessed if quasi-steady regime is reached from the initial conjectured sand levels, the convergence of the (i) sand bed morphodynamics and (ii) outgoing bulk concentration are ascertained.

As far as sand bed morphodynamics is concerned, its convergence can be assessed by quantifying the variation of the shape of the accumulated sand bed. Herein, the shape variation is estimated through the least root mean square deviation $\mathrm{LRMS}_z(t^*, t^* - \Delta t_j^*)$ between consecutive sampled sand bed surface elevations. In particular, the deviation between two consecutive profiles is minimized by means of rigid translations to retain shape deviations only (Kabsch, 1976). The LRMS deviation is then normalized with respect to the deviation range from the initial elevation of the sand bed $z_{s,0}$, so that $\Gamma_{\mathrm{LRMS}} = \mathrm{LRMS}_z(t^*, t^* - \Delta t_j^*)/[(z(t^*) - z_{s,0})_{max} - (z(t^*) - z_{s,0})_{min}]$. $\Gamma_{\mathrm{LRMS}}$ is plotted in Fig. 10 versus $t$ and $t^*$ for each sand level and test run.

The decreasing trend of $\Gamma_{\mathrm{LRMS}}$ reaches ~ 1e-2 at about $t^* \in$ [2.5e+4,3.5e+4] for each sand level and test run. This testifies that

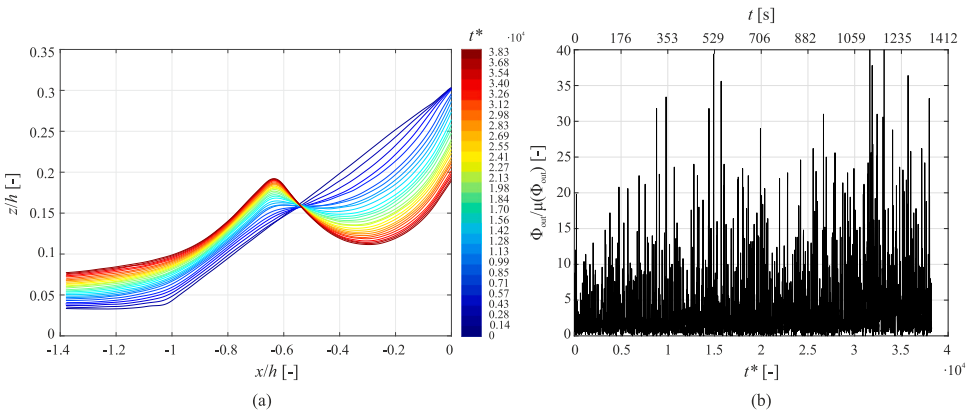


**Fig. 9.** Sand bed morphodynamic evolution (a) and outgoing bulk concentration (b) for sand level $l_1$.

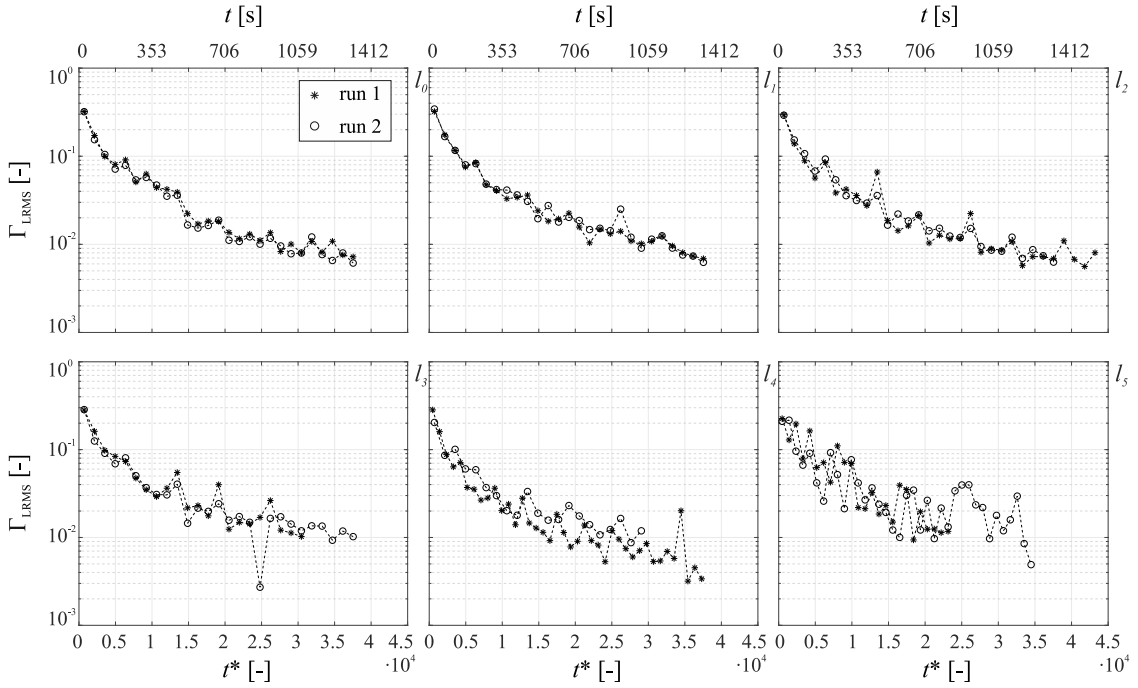


**Fig. 10.** Convergence of sand bed morphodynamics around the barrier through the evaluation of the normalized least root mean square deviation of the sand bed profile $\Gamma_{\mathrm{LRMS}}$ for each conjectured initial sand level and wind tunnel test run.

the transient regime in morphodynamics is expired and in-equilibrium conditions are essentially reached within the testing time. Overall, the obtained results demonstrate the converging time varies slightly on the conjectured initial sand level. Remarkably, the two runs show the same convergence trend for low to medium initial sand levels (from $l_0$ to $l_3$). Conversely, the repeatability of the test decreases as the initial sand level increases (see $l_4$ and $l_5$). Indeed, as the sand level increases from $l_0$ to $l_5$, a progressive increment of fluctuations can be noticed: from almost nil fluctuations for $l_0$, to heavy fluctuations for $l_5$. According to the authors, this is can be due to the technical difficulty experienced in reproducing the same conjectured sand level in both runs, especially for high levels.

As far as the outgoing sand concentration is concerned, the convergence is visually checked by means of the weighted residual $\bar{\Phi}_{res}$ of the mean value $\bar{\Phi} = \mu(\Phi)$. The weighted residual is defined for growing $t^*$ as $\bar{\Phi}_{res}(t^*) = \left|\bar{\Phi}(t^*) - \bar{\Phi}(t^* - \Delta t_k^*)\right| / \bar{\Phi}(t^*)$. The obtained results are plotted in Fig. 11 for each accumulated sand level and test run, together with the trend of residual of the mean incoming bulk concentration $\Phi_{in}$ for reference purpose.

For a fixed sand accumulation level, the two test runs show the same trend of the weighted residual. This overall confirms the overall repeatability of the test and the trustworthiness of the obtained results. $\Phi_{in}$ reaches $\bar{\Phi}_{res}$ = 1e-3 in a short time interval, i.e. $t^* \approx$ 3e+3. This is a low deviation if compared with common engineering applications. On the other hand, $\Phi_{out}$ reaches the same residual at the end of the tests at about $t^* \approx$ 4e+4. This result is in agreement with the convergence of bed morphodynamics and confirms that in-equilibrium conditions are reached for each sand level and test run. It is worth stressing that, despite the residuals of $\Phi_{in}$ and $\Phi_{out}$ differ, the rate of convergence is always $\sim 1/t^*$.

### 4.2. Bed morphodynamics and sand transport

In the following, only measurements from run 1 are retained for the sake of brevity, given the demonstrated overall repeatability of obtained results. The sand accumulation profiles are plotted in Fig. 12(a) for $t = 0$ and $t = T$. It is worth stressing that sand profiles at $t = T$ have been measured only within the FoV #1, i.e. for $-1.33 < x/H < 0$, while they are geometrically extrapolated for $x/H < -1.33$.

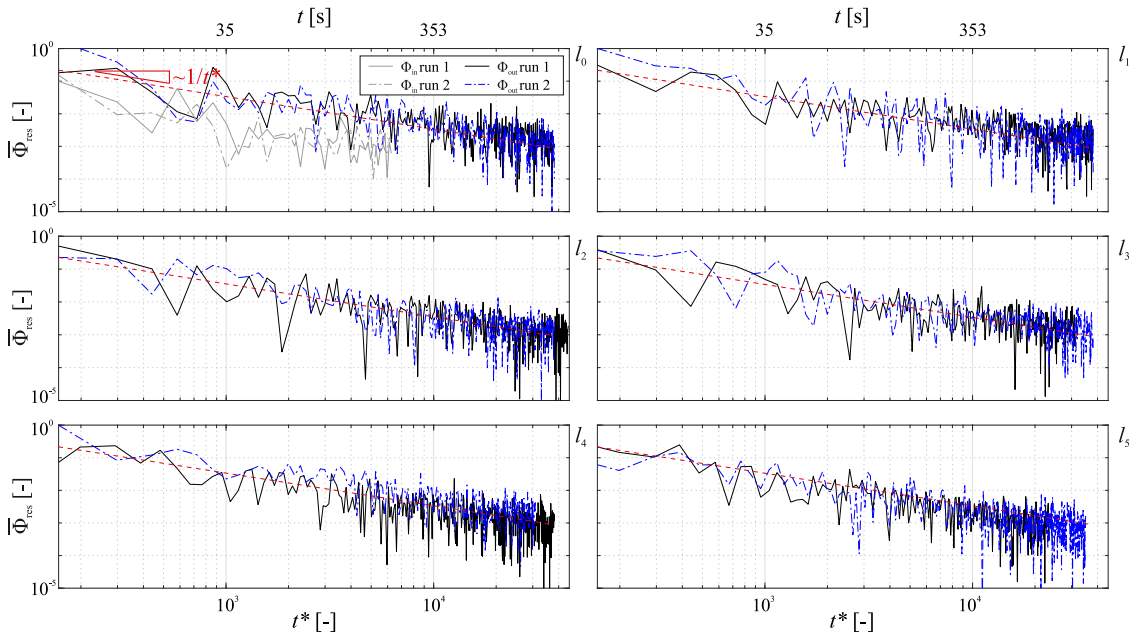


**Fig. 11.** Convergence of the mean bulk concentration $\bar{\Phi}$ through the weighted residual $\bar{\Phi}_{res}$ for each conjectured initial sand level and wind tunnel test run.

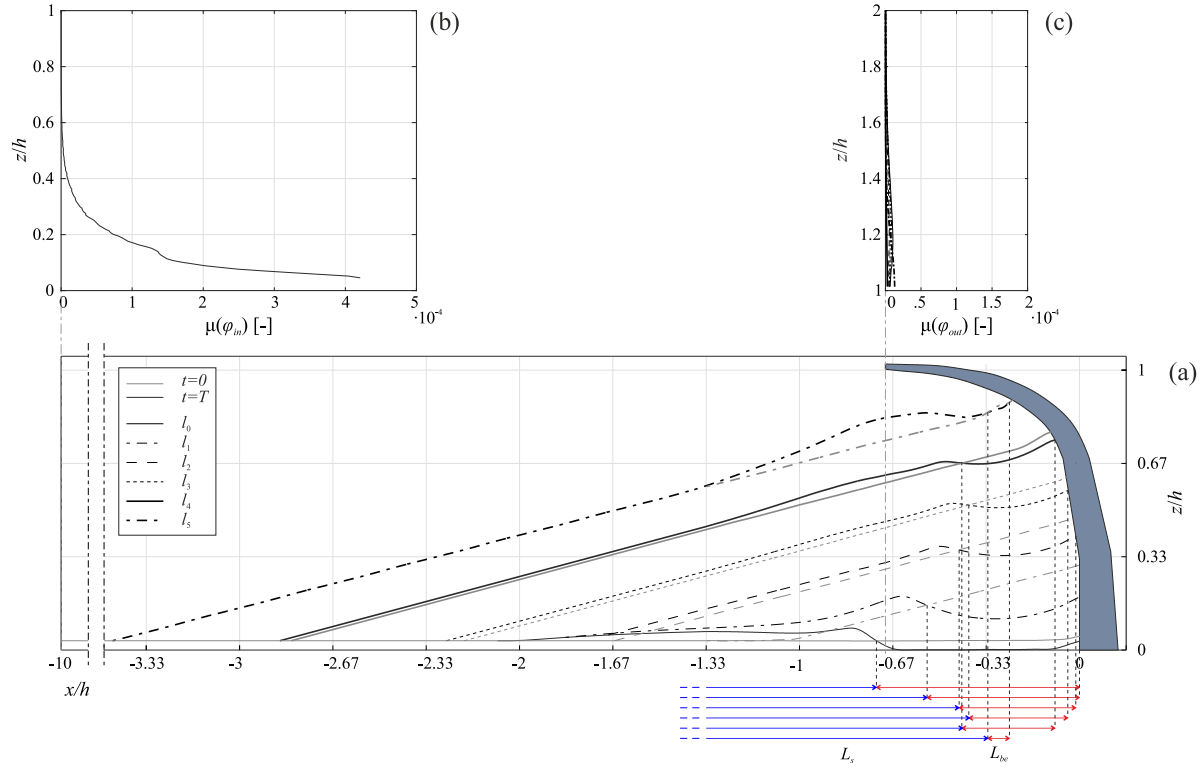


**Fig. 12.** Profiles of accumulated sand upwind the barrier at beginning and end of each test (a), incoming (b) and outgoing (c) mean sand concentration profiles for each sand level.

The sand profiles reflect the morphodynamics that takes place upwind the barrier and qualitatively confirm the working principles of S4S (Bruno et al., 2018a). On the one hand, the upwind sand trapping vortex induced by the barrier promotes backward sand erosion near the barrier. On the other hand, the barrier induces the lowering of the wind speed promoting sand sedimentation just upwind the eroded zones. The intersection between initial and final profiles splits *backward erosion zones* and *sedimentation zones*. The corresponding backward erosion lengths $L_{be}$, i.e. the horizontal length for which $u_* < -u_{*t}$, are indicated in the figure. The right boundary of the sedimentation lengths $L_s$, i.e. the horizontal length for which $u_* < |u_{*t}|$, are indicate as well within the FoV #1 for the sake of completeness. Inevitably, the upwind recirculation vortex shrinks as the sand accumulation level increases. As a result, $L_{be}$ gets necessarily shorter with increasing sand level. In particular, $L_{be} \approx 0$ for $l_5$. Nevertheless, sedimentation still holds upwind the barrier. This testifies the effectiveness of the barrier also for high levels of accumulated sand. It is worth highlighting that the acquired sand bed profiles depends on both $L_s$ and $L_{be}$, which

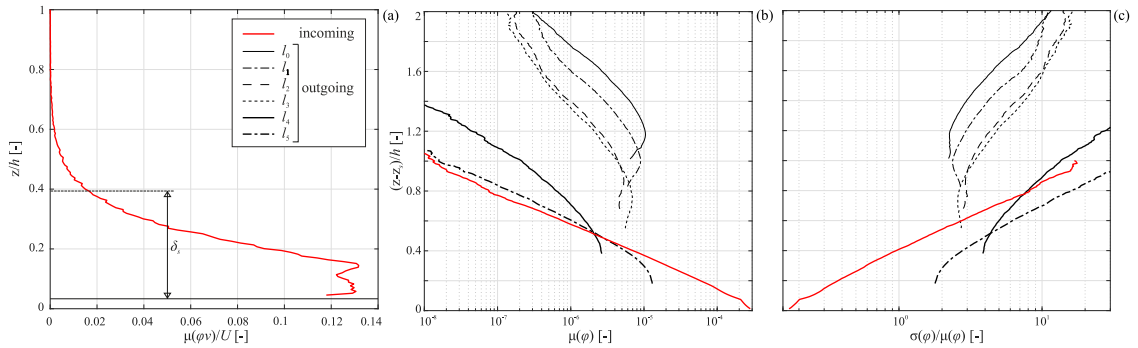


**Fig. 13.** Incoming mean sand flux profile (a), mean value (b) and coefficient of variation (c) of incoming and outgoing concentration profiles plotted versus the normalized elevation $(z - z_s)/h$ for each conjectured initial sand level.

depend in turn on the local value of the shear velocity. In particular, for fixed $z_0$, $L_s$ is expected to elongate upwind with increasing $U$, as demonstrated in Bruno et al. (2018a) in the case of nil volume of sedimented sand upwind the barrier. Accordingly, $L_{be}$ is expected to be sensitive to $U$, in turn. Indeed, the position of the separation point of the ground boundary layer upwind the barrier varies slightly because of the bluffness of the barrier. However, $L_{be}$ and $L_s$ are defined from the position of the point for which $u_*/u_{*t} = 1$, that may be expected to move upwind with increasing $U$.

Fig. 12(b,c) shows both the incoming and outgoing mean sand concentration profiles $\mu(\varphi(z)) = 1/T \int_0^T \varphi(z,t)\,dt$ for each sand accumulation level. The concentration profiles are plotted preserving the same scale in order to show their striking difference in magnitude. $\mu(\varphi_{in})$ follows a typical decreasing exponential trend (Liu and Dong, 2004). The outgoing concentration profiles are much more flattened with respect to incoming one and appear to change slightly in magnitude by varying the initial conjectured sand level.

The sand flux $q_{in}$ results from the product between the instantaneous concentration $\varphi(z,t)$ and particle velocity $v(z,t)$. The dimensionless mean incoming sand flux $\mu(\varphi(z,t)v(z,t))/U$ is plotted in Fig. 13(a). The sand flux on flat plane does not follow a typical decreasing exponential trend (Shao, 2008). However, the obtained result is consistent with some previous studies (see e.g. Dong et al., 2003). The characteristic height $\delta_s$ of the saltation layer is herein defined as the height below which 95% of the sand transport rate takes place, i.e. $\int_0^{\delta_s} \mu(q_{in}(z))\,dz / \int_0^{+\infty} \mu(q_{in}(z))\,dz = 0.95$. Therefore, it results $\delta_s/h = 0.39$, about 8 times larger with respect to typical in-field conditions.

The same concentration profiles are plotted in semi-logarithmic scale in Fig. 13(b,c) in order to highlight differences in shape among them. In particular, they are plotted versus the normalized elevation $(z - z_s)/h$, where $z_s$ is equal to the elevation of the sand bed below the trailing edge of the deflector at $t = T$ for $\varphi_{out}$ while it is equal to the upwind sand fetch height for $\varphi_{in}$. Fig. 13(b) plots the mean concentration profiles while Fig. 13(c) plots its coefficient of variation along the elevation.

For a given profile, the mean sand concentration decreases with increasing $z$, while it is the opposite for the coefficient of variation. Furthermore, $\varphi_{out}$ varies sensibly as a function of the sand accumulation levels. They can be categorized into two classes depending on their trend: (i) $l_0$, $l_1$, $l_2$, $l_3$ have a non-monotonic trend with a maximum concentration at about $(z - z_s)/h \in [0.7; 1.2]$; (ii) $l_4$ and $l_5$ have a monotonic decreasing trend, closer to the trend of $\varphi_{in}$. In fact, as the sand level increases, the profile of the outgoing concentration appears to tend to that of the incoming one. This could be due to the shrinking of the recirculation vortex and its resulting smaller effect on the vertical distribution of saltating particles. It is worth highlighting that the coefficient of variation of the outgoing concentration profiles is shifted towards high values and increases as the sand level increases, being always higher than 2. Conversely, the coefficient of variation of the incoming concentration profile covers a broad range, spanning between

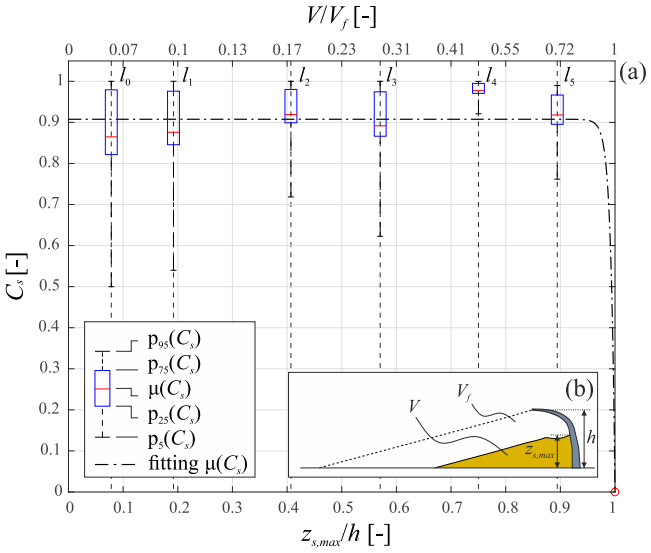


**Fig. 14.** Sedimentation coefficient of S4S model: boxplots and fitting of the mean values (a) for increasing filling height ratio $z_{s,max}/h$ and filling volume ratio $V/V_f$ (b).

0.2 and 20. This reflects the higher variability and intermittency of the outgoing concentration with respect to the incoming one, and the lower variability in concentration at lower heights.

### 4.3. Performance assessment

The mitigation performance of the S4S model are herein obtained by referring to the incoming and outgoing concentration of sand particles in air. The variability of the performance is accounted for by referring to the whole measured time series of both incoming and outgoing concentration. The performance is evaluated through the dimensionless sedimentation coefficient defined as

$$f\left(C_s\right) = \frac{f\left(\boldsymbol{\Phi}_{in}\right) - f\left(\boldsymbol{\Phi}_{out}\right)}{f\left(\boldsymbol{\Phi}_{in}\right)}, \tag{12}$$

where $f(\cdot)$ stands for the generic probability density function. $C_s$ expresses the sedimentation capability of the barrier and, given its definition, $C_s \in [0, 1]$. It is worth stressing that a high and constant $C_s$ is the design goal for Path SMMs, such as S4S. Conversely, a very low $C_s$ is preferred for other kind of obstacles on which sand sedimentation is detrimental, i.e. civil structures and infrastructures or receiver SMMs (see e.g. Raffaele and Bruno, 2019, 2020).

Fig. 14(a) shows the resulting boxplots of $C_s$ as a function of the filling height ratio $z_{s,max}/h$ and volume ratio $V/V_f$ at $t = T$, where $z_{s,max}$ is the maximum elevation of the sand bed and $V_f$ is the estimated

maximum filling capacity as sketched in Fig. 14(b). Despite the uniform linear sampling of $z_{s,max}/h$ by means of the tested six initial conditions, $V/V_f$ is not uniformly linearly sampled. On the one hand, this is because $V \propto z_{s,max}^2$, on the other hand it is difficult to correctly shape initial sand levels for $z_{s,max}/h > 0.9$. The variability of $C_s$ differs moderately among tested sand levels, resulting in a coefficient of variation in the range $\sigma(C_s)/\mu(C_s) \in [0.03, 0.21]$. In particular, the variability of $C_s$ overall decreases for increasing accumulated sand, even if the trend in non-monotonic. This suggests that the larger the upwind vortex, the larger the expected variability in $\Phi_{out}$ and $C_s$, in turn. Conversely, the mean value of $C_s$ results approximately constant by varying slightly in the range $\mu(C_s) \in [0.86, 0.97]$. According to the authors, the mean value of $C_s$ is expected to steeply decrease for $z_{s,max}/h > 0.9$ and $V/V_f > 0.7$ since $C_s$ must be nil when the barrier is completely filled of sand. The discrete mean values of $C_s$ are then fitted with the transformation of a monotonic decreasing exponential function by minimizing least squares to describe the conjectured global trend of $\mu(C_s)$. It results $\mu(C_s) = C_{s,0}(1-e^{c_1[1-(z_{s,max}/h)^{c_2}]})$, with $C_{s,0} = 0.91$, $c_1 = -26.51$, $c_2 = 4.93$. From a sand mitigation design perspective, the wind tunnel tests carried out demonstrate that S4S model traps more than 90% of the incoming sand, and that keeps high performances up to large sedimentation volumes. This implies that a very small fraction of total incoming sand can endanger the downwind protected infrastructure resulting in low frequency sand removal operations, and low related maintenance costs. Because of the conjectured dependency of the accumulated sand bed profiles on $u_*/u_{*t}$, $C_s$ may be driven not only by the ratio $V/V_f$ but also by $u_*/u_{*t}$. However, further experimental studies are required to shed some light on this issue, given the lack of results from the literature.

## 5. Conclusion

Wind-sand tunnel tests represent an effective technique to recover in a controlled environment wind-sand flow state variables and the morphodynamic evolution of the sand bed around ground-mounted obstacles. This is of paramount importance for civil structures and infrastructures in sandy environments, such as SMMs. Nevertheless, WSTTs show some deficiencies related to the lack of similarity with respect to full-scale conditions.

The present study addresses the wind-sand tunnel testing of surface-mounted obstacles by categorizing common setups and discussing wind tunnel similarity requirements from the past literature. On the one hand, the wind-sand tunnel setup, embodied by the so-called sand flux boundary conditions and sand bed initial conditions, is expected to strongly affect the trend of the measured sand state variables, e.g. the sand transport around the obstacle and the morphodynamic evolution of the sand bed. On the other hand, similarity requirements are intended to enclose any modelling scale of the windblown sand processes and, therefore, they cannot be totally fulfilled. As a result, the choice of the wind tunnel setup as well as the choice of which similarity requirements to relax shall be driven on a case-by-case basis by the aim of the study.

A case study dealing with the performance assessment of a SMM is presented and critically discussed in the wake of the adopted setup and scaling criterion. Wind tunnel testing time is shortened through the wind tunnel setup by setting proper sand bed initial conditions and running several tests in order to recover both morphodynamics and sand transport for different initial conjectured sand levels. Despite the effort to comply with similarity setup dimensionless numbers, geometric and kinematic similarity would have required the appropriate scaling of the sand grain diameter and wind speed by matching the model geometrical scaling and the Froude number, respectively. On one side, this would require the testing of dust-sized particles that would introduce additional interparticle cohesive forces, not physically sound for sand-sized particles. On the other side, the wind speed required to match the Froude number would not trigger saltation. This means that a perfect matching between model and prototype conditions remains impracticable in current WSTTs despite the adoption of large test cross-sections. This does not necessarily imply that similarity requirements should be ignored when designing wind-sand tunnel setups. Rather, the similarity between model and prototype setup dimensionless numbers should be maximized in order to minimize, in turn, the distortion between model and full-scale state variables.

The presented case study demonstrates the progressive convergence of sand bed morphodynamics and sand concentration over the barrier towards a quasi-steady state. Nevertheless, this requires long testing time: for the tested case study, the average net testing time for each sand accumulation level is equal to about 22 min. The measured sand bed morphodynamics confirms the aerodynamic working principle of the SMM highlighting that sedimentation still holds upwind the barrier even for high filling volumes. Finally, incoming and outgoing mean sand concentrations are combined to recover the dimensionless sedimentation coefficient. According to the authors, the entity of the distortion of the dimensionless sedimentation coefficient cannot be, at this stage, quantitatively assessed. However, it can be qualitatively related to the impossibility to retain the same geometrical scaling between the model, the wind speed profile, and the sand flux profile. On the one hand, the model geometry and wind speed profile can be easily scaled. On the other hand, the saltation layer cannot be scaled accordingly in the wind tunnel. As a result, the magnitude of such a distortion can be ascribed to the discrepancy, between model and prototype conditions, of the ratio between the characteristic heights of the saltation layer and the model, i.e. $\delta_s/h$. Within a modelling perspective, such a resulting dimensionless metric is considered to be analogous to another key dimensionless parameter for multiscale problems expressing the similarity of turbulence effect on structures, i.e. the ratio between the integral length scale of turbulence and the characteristic length of the model (Cook, 1978).

The above concerns are presumed to apply to any kind of tested SMM whose efficiency can be affected by $\delta_s/h$. In particular, porous fences constitute another class of popular Path SMM (Li and Sherman, 2015; Lima et al., 2020). Despite WSTTs on porous fences are widespread, the authors expect that they give rise to even greater experimental distortion. Indeed, pure aerodynamic scaling is particularly critical for porous obstacles (Allori et al., 2013). In addition, geometric scaling is expected to be crucial given the emergence of the pore diameter as an additional characteristic length scale of the problem. Overall, porosity overcomplicates physical similarity between modelled and full-scale conditions and highlights once again the incompatibility between kinematic and geometric similarities.

In the light of the wide research field, we suggest the following research perspectives to the whole scientific community in order to fill the gaps of knowledge emerged by the present study. First, we would like to promote further WSTTs to explore the sand sedimentation pattern and trapping performance under different geometrical scaling of the model and environmental setup conditions, e.g. wind yaw angle, effective shear velocity, and wind flow features, i.e. Reynolds and Froude number. Secondly, given the emerged practical limitations of WSTTs in complying with similarity requirements, we strongly encourage the quantification of experimental distortion of different kind of SMMs in a hybrid modelling perspective (Meroney, 2016) by recurring to supplementary wind tunnel tests in open jet large scale facilities, such as Wall of Wind (Gan Chowdhury et al., 2017), and complementary computational simulations relying on multiphase models of windblown sand transport coupled with morphodynamic evolution (e.g. Lo Giudice and Preziosi, 2020). The hybrid physical-computational modelling can be beneficial for a wide range of studies all related to windblown sand modelling, ranging from SMM performance assessment (HyPer SMM, 2020) to, in an even broader perspective, the investigation of windblown sand transport on martian and other extraterrestrial planetary surfaces (Rasmussen et al., 2015).

## CRediT authorship contribution statement

**Lorenzo Raffaele:** Conceptualization, Methodology, Formal analysis, Writing - original draft, Writing - review & editing. **Jeroen van Beeck:** Methodology, Writing - review & editing. **Luca Bruno:** Conceptualization, Methodology, Writing - review & editing.

## Acknowledgements

The study is part of the MSCA-IF-2019 research project Hybrid Performance Assessment of Sand Mitigation Measures (HyPer SMM). This project has received funding from the European Union's Horizon 2020 research and innovation programme under the Marie Sklodowska-Curie grant agreement No. 885985. In particular, we acknowledge G. Glabeke and S. Porchetta from von Karman Institute for Fluid Dynamics for their involvement in wind tunnel tests. Wind tunnel tests have been accomplished within the "Proof of Concept" programme of Politecnico di Torino, funded by Compagnia di San Paolo. The experimental campaign has been developed in the framework of the Windblown Sand Modelling and Mitigation (WSMM) joint research, development and consulting group established between Politecnico di Torino and Optiflow Company.

## Declaration of competing interest

The authors declare that they have no known competing financial interests or personal relationships that could have appeared to influence the work reported in this paper.

## References

Alghamdi, A.A., Al-Kahtani, N.S., 2005. Sand control measures and sand drift fences. J. Perform. Constr. Facil. 19, 295–299. http://dx.doi.org/10.1061/(ASCE)0887-3828(2005)19:4(295).

Allori, D., Bartoli, G., Mannini, C., 2013. Wind tunnel tests on macro-porous structural elements: A scaling procedure. J. Wind Eng. Ind. Aerodyn. 123, 291–299. http://dx.doi.org/10.1016/j.jweia.2013.09.011.

Anno, Y., 1984. Requirements for modeling of a snowdrift. Cold Reg. Sci. Technol. 8, 241–252. http://dx.doi.org/10.1016/0165-232X(84)90055-7.

Bagnold, R.A., 1941. The physics of blown sand and desert dunes. Methuen http://dx.doi.org/10.1007/978-94-009-5682-7.

Blocken, B., Stathopoulos, T., van Beeck, J., 2016. Pedestrian-level wind conditions around buildings: Review of wind-tunnel and CFD techniques and their accuracy for wind comfort assessment. Build. Environ. 100, 50–81. http://dx.doi.org/10.1016/j.buildenv.2016.02.004.

Blocken, B., Stathopoulos, T., Carmeliet, J., 2007. CFD simulation of the atmospheric boundary layer: wall function problems. Atmos. Environ. 41, 238–252. http://dx.doi.org/10.1016/j.atmosenv.2006.08.019.

Bofah, K.K., Al-Hinai, K.G., 1986. Field tests of porous fences in the regime of sand-laden wind. J. Wind Eng. Ind. Aerodyn. 23, 309–319. http://dx.doi.org/10.1016/0167-6105(86)90051-6.

Bruno, L., Fransos, D., L. Giudice, A., 2018a. Solid barriers for windblown sand mitigation: Aerodynamic behavior and conceptual design guidelines. J. Wind Eng. Ind. Aerodyn. 173, 79–90. http://dx.doi.org/10.1016/j.jweia.2017.12.005.

Bruno, L., Horvat, M., Raffaele, L., 2018b. Windblown sand along railway infrastructures: A review of challenges and mitigation measures. J. Wind Eng. Ind. Aerodyn. 177, 340–365. http://dx.doi.org/10.1016/j.jweia.2018.04.021.

Bruno, L., Preziosi, L., Fransos, D., 2016. A deflecting module for an anti-sand barrier, a barrier thus obtained and a protection method from windblown sand. WO 2016/181417 A1.

Carneiro, M.V., Rasmussen, K.R., Herrmann, H.J., 2015. Bursts in discontinuous aeolian saltation. Sci. Rep. 11109. http://dx.doi.org/10.1038/srep11109.

Charnock, H., 1955. Wind stress on a water surface. Q. J. R. Meteorol. Soc. 81, 639–640. http://dx.doi.org/10.1002/qj.49708135027.

Chen, B., Cheng, J., Xin, L., Wang, R., 2019. Effectiveness of hole plate-type sand barriers in reducing aeolian sediment flux: Evaluation of effect of hole size. Aeolian Res. 38, 1–12. http://dx.doi.org/10.1016/j.aeolia.2019.03.001.

Cheng, J., Xin, G., Zhi, L., Jiang, F., 2017. Unloading characteristics of sand-drift in wind-shallow areas along railway and the effect of sand removal by force of wind. Sci. Rep. 7 (41462), http://dx.doi.org/10.1038/srep41462.

Cook, N.J., 1978. Determination of the model scale factor in wind-tunnel simulations of the adiabatic atmospheric boundary layer. J. Wind Eng. Ind. Aerodyn. 2, 311–321. http://dx.doi.org/10.1016/0167-6105(78)90016-8.

Delpech, P., Palier, P., Gandemer, J., 1998. Snowdrifting simulation around antarctic buildings. J. Wind Eng. Ind. Aerodyn. 74–76, 567–576. http://dx.doi.org/10.1016/S0167-6105(98)00051-8.

Dong, Z., Liu, X., Wang, H., Zhao, A., Wang, X., 2003. The flux profile of a blowing sand cloud: a wind tunnel investigation. Geomorphology 49, 219–230. http://dx.doi.org/10.1016/S0169-555X(02)00170-8.

EN 1991-1-4, 1991. Eurocode 1: Actions on structures - Part 1-4: General actions - Wind actions. EN 1991-1-4.

Faria, R., Ferreira, A.D., Sismeiro, J.L., Mendes, J.C.F., Sousa, A.C.M., 2011. Wind tunnel and computational study of the stoss slope effect on the aeolian erosion of transverse sand dunes. Aeolian Res. 3, 303–314. http://dx.doi.org/10.1016/j.aeolia.2011.07.004.

Farrell, E.J., Sherman, D.J., 2015. A new relationship between grain size and fall (settling) velocity in air. Prog. Phys. Geogr. 39, 361–387. http://dx.doi.org/10.1177/0309133314562442.

Ferreira, A.D., Fino, M.R.M., 2012. A wind tunnel study of wind erosion and profile reshaping of transverse sand piles in tandem. Geomorphology 139–140, 230–241. http://dx.doi.org/10.1016/j.geomorph.2011.10.024.

Gan Chowdhury, A., Zisis, I., Irwin, P., Bitsuamlak, G., 2017. Downloaded 799 timestechnical paperslarge-scale experimentation using the 12-fan wall of wind to assess and mitigate hurricane wind and rain impacts on buildings and infrastructure systems. J. Struct. Eng. 143, http://dx.doi.org/10.1061/(ASCE)ST.1943-541X.0001785.

Greeley, R., Iversen, J.D., Pollack, J.B., Udovich, N., White, B., 1974. Wind tunnel studies of Martial aeolian processes. Proc. R. Soc. A 341, http://dx.doi.org/10.1098/rspa.1974.0191.

Ho, T.D., Valance, A., Dupont, P., Olud E. Moctar, A., 2014. Aeolian sand transport: Length and height distributions of saltation trajectories. Aeolian Res. 12, 65–74. http://dx.doi.org/10.1016/j.aeolia.2013.11.004.

Horvat, M., Bruno, L., Khris, S., Raffaele, L., 2020. Aerodynamic shape optimization of barriers for windblown sand mitigation using cfd analysis. J. Wind Eng. Ind. Aerodyn. 197, 104058. http://dx.doi.org/10.1016/j.jweia.2019.104058.

Hotta, S., Horikawa, K., 1991. Function of sand fence placed in front of embankment. Coast. Eng. 1990 (2), 2754–2767. http://dx.doi.org/10.1061/9780872627765.211.

HyPer SMM, 2020. HyPer SMM - hybrid performance assessment of sand mitigation measures, H2020-MSCA-IF-2019. URL https://hypersmm.vki.ac.be/.

Isyumov, N., 1971. An Approach To the Prediction of Snow Loads (Ph.D. thesis).

Isyumov, N., Mikitiuk, M., 1990. Wind tunnel model tests of snow drifting on a two-level flat roof. J. Wind Eng. Ind. Aerodyn. 36 (Part 2), 893–904. http://dx.doi.org/10.1016/0167-6105(90)90086-R.

Iversen, J.D., 1980. Drifting-snow similitude—transport-rate and roughness modeling. J. Glaciol. 26, 393–403. http://dx.doi.org/10.3189/S0022143000010923.

Iversen, J.D., 1981. Comparison of wind-tunnel model and full-scale snow fence drifts. J. Wind Eng. Ind. Aerodyn. 8, 231–249. http://dx.doi.org/10.1016/0167-6105(81)90023-4.

Iversen, J.D., Wang, W., Rasmussen, K.R., Mikkelsen, H.E., Hasiuk, J.F., Leach, R.N., 1990. The effect of a roughness element on local saltation transport. J. Wind Eng. Ind. Aerodyn. 36 (Part 2), 845–854. http://dx.doi.org/10.1016/0167-6105(90)90081-M.

Jensen, M., 1958. The model law for phenomena in the natural wind. Ingenioren 2, 121–128.

Jiang, H., Huang, N., Zhu, Y., 2014. Analysis of wind-blown sand movement over transverse dunes. Sci. Rep. 4 (7114), http://dx.doi.org/10.1038/srep07114.

Kabsch, W., 1976. A solution for the best rotation to relate two sets of vectors. Acta Crystallogr. A 32, 922–923. http://dx.doi.org/10.1107/S0567739476001873.

Kerr, R.C., Nigra, J.O., 1952. Eolian sand control. Bull. Am. Assoc. Pet. Geol. 36, 1541–1573.

Kind, R.J., 1976. A critical examination of the requirements for model simulation of wind-induced erosion/deposition phenomena such as snow drifting. Atmos. Environ. 10, 219–227. http://dx.doi.org/10.1016/0004-6981(76)90094-9.

Kind, R.J., 1986. Snowdrifting: A review of modelling methods. Cold Reg. Sci. Technol. 12, 217–228. http://dx.doi.org/10.1016/0165-232X(86)90036-4.

Kok, J.F., Parteli, E.J.R., Michaels, T.I., Karam, D.B., 2012. The physics of wind-blown sand and dust. Rep. Progr. Phys. 75, 106901. http://dx.doi.org/10.1088/0034-4885/75/10/106901.

Kwok, K.C.S., Kim, D.H., Smedley, D.J., Rohde, H.F., 1992. Snowdrift around buildings for antarctic environment. J. Wind Eng. Ind. Aerodyn. 44, 2797–2808. http://dx.doi.org/10.1016/0167-6105(92)90073-J.

Lancaster, N., 1995. Geomorphology of Desert Sand Dunes. Routledge, Cambridge, England, http://dx.doi.org/10.4324/9780203413128.

Li, B., Sherman, D.J., 2015. Aerodynamics and morphodynamics of sand fences: A review. Aeolian Res. 17, 33–48. http://dx.doi.org/10.1016/j.aeolia.2014.11.005.

Lima, I.A., Parteli, E.J.R., Shao, Y., Andrade, J.S., Herrmann, H.J., Araújo, A.D., 2020. Cfd simulation of the wind field over a terrain with sand fences: Critical spacing for the wind shear velocity. Aeolian Res. 43, 100574. http://dx.doi.org/10.1016/j.aeolia.2020.100574.

Liu, X., Dong, Z., 2004. Experimental investigation of the concentration profile of a blowing sand cloud. Geomorphology 60, 371–381. http://dx.doi.org/10.1016/j.geomorph.2003.08.009.

Liu, M., Zhang, Q., Fan, F., Shen, S., 2018. Experiments on natural snow distribution around simplified building models based on open air snow-wind combined experimental facility. J. Wind Eng. Ind. Aerodyn. 173, 1–13. http://dx.doi.org/10.1016/j.jweia.2017.12.010.

Lo Giudice, A., Nuca, R., Preziosi, L., Coste, N., 2019. Wind-blown particulate transport: A review of computational fluid dynamics models. Math. Eng. 1, 508–547. http://dx.doi.org/10.3934/mine.2019.3.508.

Lo Giudice, A., Preziosi, L., 2020. A fully eulerian multiphase model of windblown sand coupled with morphodynamic evolution: Erosion, transport, deposition, and avalanching. Appl. Math. Model. 79, 68–84. http://dx.doi.org/10.1016/j.apm.2019.07.060.

Luo, W., Lu, J., Qian, G., Dong, Z., 2016. Influence of the gap ratio on variations in the surface shear stress and on sand accumulation in the lee of two side-by-side obstacles. Environ. Earth Sci. 75, 766. http://dx.doi.org/10.1007/s12665-016-5588-3.

Martin, R.L., Kok, J.F., 2017. Wind-invariant saltation heights imply linear scaling of aeolian saltation flux with shear stress. Sci. Adv. 3, e1602569. http://dx.doi.org/10.1126/sciadv.1602569.

McKenna Neuman, C., 2003. Effects of temperature and humidity upon the entrainment of sedimentary particles by wind. Bound. Layer Meteorol. 108, 61–89. http://dx.doi.org/10.1023/A:1023035201953.

McKenna Neuman, C., Bédard, O., 2015. A wind tunnel study of flow structure adjustment on deformable sand beds containing a surface-mounted obstacle. J. Geophys. Res.: Earth Surf. 120, 1824–1840. http://dx.doi.org/10.1002/2015JF003475.

Meroney, R.N., 2016. Ten questions concerning hybrid computational/physical model simulation of wind flow in the built environment. Build. Environ. 96, 12–21. http://dx.doi.org/10.1016/j.buildenv.2015.11.005.

Middleton, N.J., Sternberg, T., 2013. Climate hazards in drylands: A review. Earth-Sci. Rev. 126, 48–57. http://dx.doi.org/10.1016/j.earscirev.2013.07.008.

Mochizuki, H., Okada, Y., Kumar, S., Sinha, S., 2012. Investigation into sand movement around a column using a wind tunnel. J. Arid Land Stud. 22, 267–270.

Odar, F., 1965. Simulation of Drifting Snow. Research Report 174, U.S. Army Cold Regions Research and Engineering Laboratory.

Owen, P.R., 1964. Saltation of uniform grains in air. J. Fluid Mech. 20, 225–242. http://dx.doi.org/10.1017/S0022112064001173.

Owen, P.R., Gillette, D., 1985. Wind tunnel constraint on saltation. In: Proc. International Workshop on the Physics of Blown Sand. University of Aarhys, Denmark, pp. 253–269.

Pähtz, T., Kok, J.F., Herrmann, H.J., 2012. The apparent roughness of a sand surface blown by wind from an analytical model of saltation. New J. Phys. 14, 043035. http://dx.doi.org/10.1088/1367-2630/14/4/043035.

Pähtz, T., Liu, Y., Xia, Y., Hu, P., He, Z., Tholen, K., 2021. Unified model of sediment transport threshold and rate across weak and intense subaqueous bedload, windblown sand, and windblown snow. J. Geophys. Res.: Earth Surf. 126, http://dx.doi.org/10.1029/2020JF005859, e2020JF005859.

Peterka, J.A., Petersen, R.L., 1990. On the relaxation of saltation length as a modelingcriteria for particulate transport by wind. J. Wind Eng. Ind. Aerodyn. 36, 867–876. http://dx.doi.org/10.1016/0167-6105(90)90083-O.

Qiang, S., Zhou, X., Kosugi, K., Gu, M., 2019. A study of snow drifting on a flat roof during snowfall based on simulationsin a cryogenic wind tunnel. J. Wind Eng. Ind. Aerodyn. 188, 269–279. http://dx.doi.org/10.1016/j.jweia.2019.02.022.

Raffaele, L., Bruno, L., 2019. Windblown sand action on civil structures: Definition and probabilistic modelling. Eng. Struct. 178, 88–101. http://dx.doi.org/10.1016/j.engstruct.2018.10.017.

Raffaele, L., Bruno, L., 2020. Windblown sand mitigation along railway megaprojects: A comparative study. Struct. Eng. Int. 30, 355–364. http://dx.doi.org/10.1080/10168664.2020.1714530.

Raffaele, L., Bruno, L., Pellerey, F., Preziosi, L., 2016. Windblown sand saltation: A statistical approach to fluid threshold shear velocity. Aeolian Res. 23, 79–91. http://dx.doi.org/10.1016/j.aeolia.2016.10.002.

Raffaele, L., Bruno, L., Sherman, D.J., 2020. Statistical characterization of sedimentation velocity of natural particles. Aeolian Res. 44, 100593. http://dx.doi.org/10.1016/j.aeolia.2020.100593.

Rasmussen, K.R., Valance, A., Merrison, J., 2015. Laboratory studies of aeolian sediment transport processes on planetary surfaces. Geomorphology 244, 74–94. http://dx.doi.org/10.1016/j.geomorph.2015.03.041.

Redding, J.H., Lord, J.A., 1981. Designing for the effects of windblown sand along the new Jessah-Riyadh-Dammam expressway, in: Symposium on Geotechnical Problems in Saudi Arabia, pp. 363–395.

Rizvi, A.A., 1989. Planning responses to aeolian hazards in arid regions. J. King Saud Univ. Archit. Plan. 1, 59–74.

Rodrigo, J.S., van Beeck, J., Buchlin, J.M., 2012. Wind engineering in the integrated design of princess elisabeth antarctic base. Build. Environ. 52, 1–18. http://dx.doi.org/10.1016/j.buildenv.2011.12.023.

Shao, Y., 2008. Physics and Modelling of Wind Erosion. Springer, http://dx.doi.org/10.1007/978-1-4020-8895-7.

Shao, Y., Lu, H., 2000. A simple expression for wind erosion threshold friction velocity. J. Geophys. Res.: Atmos. 105, 22437–22443. http://dx.doi.org/10.1029/2000JD900304.

Shao, Y., Raupach, M.R., 1992. The overshoot and equilibration of saltation. J. Geophys. Res.: Atmos. 97, 20559–20564. http://dx.doi.org/10.1029/92JD02011.

Sherman, D.J., 2020. Understanding wind-blown sand: Six vexations. Geomorphology 366, 107193. http://dx.doi.org/10.1016/j.geomorph.2020.107193.

Sherman, D.J., Farrell, E.J., 2008. Aerodynamic roughness lengths over movable beds: Comparison of wind tunnel and field data. J. Geophys. Res.: Earth Surf. 113, F02S08. http://dx.doi.org/10.1029/2007JF000784.

Simiu, E., Scanlan, R.H., 1996. Winds Effects on Structures: Fundamentals and Applications To Design, third ed. Wiley, New York.

Snyder, W.H., 1972. Similarity criteria for the application of fluid models to the study of air pollution meteorology. Bound.-Lay. Meteorol. 3, 113–134. http://dx.doi.org/10.1007/BF00769111.

Storm, G., Kelly, G.R., Keitz, E.L., Weiss, R.F., 1962. Scale model studies on snow drifting.

Tominaga, Y., 2018. Computational fluid dynamics simulation of snowdrift around buildings: Past achievements and future perspectives. Cold Reg. Sci. Technol. 150, 2–14. http://dx.doi.org/10.1016/j.coldregions.2017.05.004.

Tominaga, Y., Okaze, T., Mochida, A., 2018. Wind tunnel experiment and cfd analysis of sand erosion/deposition due to wind around an obstacle. J. Wind Eng. Ind. Aerodyn. 182, 262–271. http://dx.doi.org/10.1016/j.jweia.2018.09.008.

Tominaga, Y., Stathopoulos, T., 2020. CFD simulations can be adequate for the evaluation of snow effects on structures. Build. Simul. 13, 729–737. http://dx.doi.org/10.1007/s12273-020-0643-0.

Tsukahara, T., Sakamoto, Y., Aoshima, D., Yamamoto, M., Kawaguchi, Y., 2012. Visualization and laser measurements on the flow field and sand movement on sand dunes with porous fences. Exp. Fluids 52, 877–890. http://dx.doi.org/10.1007/s00348-011-1157-4.

Wang, T., Qu, J., Ling, Y., Liu, B., Xiao, J., 2018. Shelter effect efficacy of sand fences: A comparison of systems in a wind tunnel. Aeolian Res. 30, 32–40. http://dx.doi.org/10.1016/j.aeolia.2017.11.004.

Wang, T., Qu, J., Ling, Y., Xie, S., Xiao, J., 2017. Wind tunnel test on the effect of metal net fences on sand flux in a Gobi Desert, China. J. Arid Land 9, 888–899. http://dx.doi.org/10.1007/s40333-017-0068-5.

Wang, X.M., Zhang, C.X., Hasi, E., Dong, Z.B., 2010. Has the Three Norths Forest Shelterbelt Program solved the desertification and dust storm problems in arid and semiarid China?. J. Arid Environ. 74, 13–22. http://dx.doi.org/10.1016/j.jaridenv.2009.08.001.

White, B.R., 1996. Laboratory simulation of aeolian sand transport and physical modeling of flow around dunes. Ann. Arid Zone 35, 187–213.

White, B.R., Mounla, H., 1991. An experimental study of Froude number effect on wind-tunnel saltation. Acta Mech. 1, 145–157. http://dx.doi.org/10.1007/978-3-7091-6706-9_9.

Xiao, J., Yao, Z., Qu, J., 2015. Influence of golmud-lhasa section of Qinghai–Tibet railway on blown sand transport. Chin. Geogr. Sci. 25, 39–50. http://dx.doi.org/10.1007/s11769-014-0722-1.

Zhang, N., Kang, J.H., Lee, S.J., 2010. Wind tunnel observation on the effect of a porous wind fence on shelter of saltating sand particles. Geomorphology 120, 224–232. http://dx.doi.org/10.1016/j.geomorph.2010.03.032.

Zhang, K., Qu, J., Han, Q., Xie, S., Kai, K., Niu, Q., An, Z., 2014. Wind tunnel simulation of windblown sand along China's Qinghai-Tibet railway. Land Degradation Dev. 25, 244–250. http://dx.doi.org/10.1002/ldr.2137.

Zhang, C.L., Zou, X.Y., Cheng, H., Yang, S., Pan, X.H., Liu, Y.Z., Dong, G.R., 2007. Engineering measures to control windblown sand in Shiquanhe Town, Tibet. J. Wind Eng. Ind. Aerodyn. 95, 53–70. http://dx.doi.org/10.1016/j.jweia.2006.05.006.

Zhou, X., Hu, J., Gu, M., 2014. Wind tunnel test of snow loads on a stepped flat roof using different granular materials. Nat. Hazards 74, 1629–1648. http://dx.doi.org/10.1007/s11069-014-1296-z.

Zingg, A.W., 1953. Wind tunnel studies of the movement of sedimentary material. In: Proceedings of the 5th Hydraulic Conference Bulletin. Inst. of Hydraulics, Iowa City, pp. 111–135.